

UNIVERSITY OF WARWICK
SCHOOL OF ENGINEERING

Warwick Mobile Robotics: Urban Search and Rescue Robot

ES410 Group Project Technical Report

02/05/2013

Authors:

Kristian Buckstone
Lewis Judd
Nicholas Orłowski
Michael Tayler-Grint
Rachele Williams
Edgars Zauls



a tti company

maxon motor

driven by precision



School of Engineering
The University of Warwick

The Vice Chancellor
The University of Warwick

Abstract

Urban Search and Rescue (USAR) robots are designed to locate survivors in hazardous environments such as earthquake zones. The Warwick Mobile Robotics (WMR) team has enhanced a prototype USAR robot with the aims of:

- Entering the World RoboCup Rescue competition
- Improving the prototype's commercial viability by eliminating key weaknesses in the current design

WMR 2012/2013 has been working to address key weaknesses in the tele-operated robot design. The system's reliability has been improved by redesigning the chassis and head to reduce vibrations and eliminating recurring problems in the electronics. Additionally, system safety has been increased by developing an easy-to-use battery-pack.

Reuse of existing sensors has increased operator awareness and been a cost-effective way to markedly improve robot tele-operation performance. This was also boosted by a revamped controller layout and GUI, which allows the operator to fully utilise the newly-developed inverse kinematic capabilities.

A full-system test in a realistic outdoors scenario has been carried out at Northrop Grumman Remotec's facility. On this basis good performance is predicted in the 2013 World RoboCup Rescue championship in Eindhoven.

Table of Contents

1	Introduction.....	1
2	Background to the WMR Project.....	1
2.1	Motivation for Development of Search and Rescue Robotics	1
2.2	Commercial Competition	2
2.3	World RoboCup Competition 2013	4
3	Product Development Strategy	6
3.1	Requirement Analysis.....	6
3.2	SWOT Analysis	8
3.3	WMR 2012/2013 Objectives	9
4	Chassis	10
4.1	Initial State.....	10
4.2	Specification	11
4.3	Chassis Redesign.....	11
4.4	Shell Design	22
4.5	Results	23
5	Power System.....	24
5.1	Introduction.....	24
5.2	Battery Enclosure	24
5.3	Battery Monitoring.....	27
5.4	Power Board	29
5.5	Wiring	31
6	Sensors and Devices	33
6.1	Initial State.....	33
6.2	Specification	36
6.3	Actions.....	36

6.4	Results	43
7	Control system.....	44
7.1	Initial State.....	44
7.2	Specification	45
7.3	Architecture.....	45
7.4	Graphical User Interface.....	47
7.5	Collision System and Error Checking	48
7.6	3D Representation.....	50
7.7	Arm Control	53
7.8	Controller Layout.....	58
8	Testing	60
8.1	Aims	60
8.2	Method	60
8.3	Results	61
8.4	Analysis of Results	70
9	Critical Review	72
10	Conclusions.....	75
11	References.....	76
	Appendices	82
	Appendix A: Chassis supporting data and calculations	82
	Appendix B: Power System support materials	96
	Appendix C: Sensors & devices supporting data	97
	Appendix D: Control system support materials	99
	Appendix E: Other support materials.....	105

1 Introduction

Urban Search and Rescue (USAR) robots are designed to locate survivors in hazardous environments such as earthquake zones. This reduces the risk a human rescue team is exposed to and allows them to plan the rescue more effectively.

The Warwick Mobile Robotics (WMR) project has developed a prototype USAR robot. This year the team's aims are:

- Enter the World RoboCup Rescue competition, building on previous teams' successes at the European level.
- Improve the commercial viability of the prototype by eliminating key weaknesses in the current design.

2 Background to the WMR Project

2.1 Motivation for Development of Search and Rescue Robotics

Several recent disasters have highlighted the need for search and rescue robots, such as:

- The 2010 Chilean mining accident where 33 men were trapped underground (Franklin 2010)
- The 2011 Fukushima Accident where a tsunami caused destruction to a nuclear power plant (World Nuclear Association 2013)

The main advantages to using robots in such situations are (Tadokoro 2009):

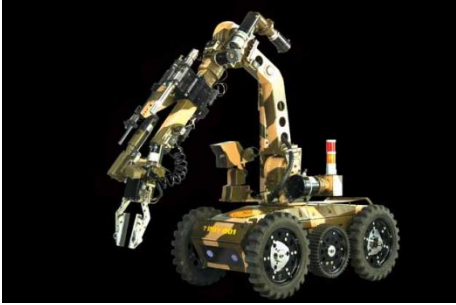

1. Robots can operate in conditions that humans cannot, locating survivors that would have died otherwise.
2. Robots can fit through confined spaces, reducing or eliminating the risk of secondary damage caused by excavating access routes.
3. Using robots can accelerate rescue operations, increasing the chance of finding survivors.

The WMR team recognises the vital contribution of robots to search and rescue operations and intends to bring the existing design closer to real-world deployment.

2.2 Commercial Competition

USAR robots must be mobile and benefit from having a manipulator and a range of sensors. Bomb disposal robots have similar requirements. Some commercial robots in both of these markets are outlined in Table 1.

Table 1. Competitor analysis

Market	Commercial Competitor
Bomb Disposal	<p>DRDO – Daksh (Press Trust of India 2011)</p> <ul style="list-style-type: none"> • Battery-powered, teleoperated, wheeled robot (Figure 1). • Main features: manipulator arm, X-ray scanner, water jet disrupter, shotgun (for breaching locked doors).  <p>Figure 1. DRDO Daksh.</p>
	<p>Northrop Grumman Remotec – ANDROS F6A (Northrop Grumman 2013)</p> <ul style="list-style-type: none"> • Battery-powered, teleoperated, tracked robot (Figure 2). • Main features: multiple video cameras, manipulator arm with a range of tools and accessories.  <p>Figure 2. Remotec ANDROS F6-A</p>

**Disaster
Search
and
Rescue**

Tokyo Fire Department – RoboCue (Nosowitz 2011)

- Battery-powered, teleoperated, tracked robot (Figure 3).
- Function: evacuate casualties from danger-zone.
- Main features: ultrasonic sensors, infrared cameras, on-board oxygen canister.



Figure 3. RoboCue lifting a victim (Nosowitz 2011)

Satoshi Tadokoro – Snakebot (Diginfonews 2008)

- Electrically-powered, teleoperated, cilia-actuated robot (Figure 4).
- Function: deep-penetration fiberscope.
- Main features: nylon bristles, light, speaker.

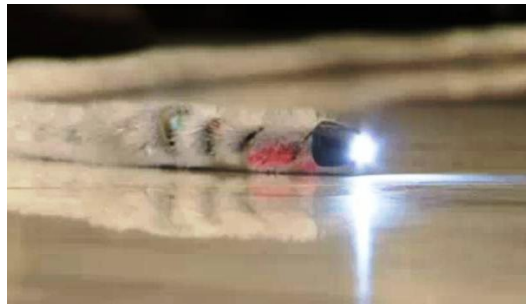


Figure 4. Snakebot

VECNA Solutions – BEAR (VECNA 2013)

- Battery-powered, teleoperated, tracked (Figure 5).
- Function: heavy lifting over rough terrain.
- Main features: hydraulic upper-body, reconfigurable track “legs”, versatile manipulator arms.



Figure 5. Visualisation of BEAR Medic-Bot

It can be seen that most commercial solutions are battery-powered, teleoperated and tracked much like WMR's prototype.

2.3 World RoboCup Competition 2013



The RoboCup Rescue competition is an independent event that allows USAR robots to be compared based on their performance. The competition is based around a simulated disaster zone through which robots must navigate in order to find victims. Points are awarded for each victim discovered as well as for other abilities such as mapping and manipulation.

For the last five years, WMR has attended the European competition in Germany. Since the robot has performed consistently well at this level the team has decided to attend the World competition this year.

2.3.1 RoboCup Competitor Analysis

The two best teams from the 2012 World competition are listed in Table 2 as examples of the world-class robots that WMR seeks to compete against.

Table 2. Top performing robots in recent World RoboCup competitions.

Competitor Team	Types of robots used	Key Features of main competitor robot	Sensors	System Cost
<p>MRL (Iran)</p>  <p>Figure 6. NAJI-VII robot (Shahri et al, 2012)</p>	<p>Three:</p> <ul style="list-style-type: none"> • Autonomous • Teleoperated (Figure 6) • Flying 	<ul style="list-style-type: none"> • Motor outputs are coupled in pairs for increased power. • 6 degree of freedom (DoF) manipulator arm. (Shahri, et al. 2011) 	<p>CO₂ sensor, inertial measurement unit (IMU), LiDAR, motor encoders, sonar, thermal camera, video cameras</p>	<p>£6000-£10000</p>
<p>Hector Darmstadt (Germany)</p>  <p>Figure 7. Hector GV robot (Hector Darmstadt, 2012)</p>	<p>Three:</p> <ul style="list-style-type: none"> • Autonomous (Figure 7) • Flying • Marine 	<ul style="list-style-type: none"> • 4 wheel drive and steering (Hector Darmstadt 2012) • Vision system for hazmat symbol and victim identification. 	<p>CO₂ sensor, IMU, LiDAR, microphone, motor encoders, sonar, thermal camera, X-Box Kinect (Graber, et al. 2011)</p>	<p>£12000</p>

It can be seen that both teams have multiple robots. Of the two teams' robots, WMR's design is most similar to the NAJI-VII.

3 Product Development Strategy

As outlined in the Introduction, the WMR team’s aims were to enter the World RoboCup Rescue competition and improve the commercial viability of the prototype. The design process used to achieve these aims is shown in Figure 8.

Requirements to achieve the aims were linked to strengths and weaknesses of the original prototype and objectives which provided the largest benefit for the effort required were given priority. Each sub-system had a specification and test-plan written based on the objectives chosen.

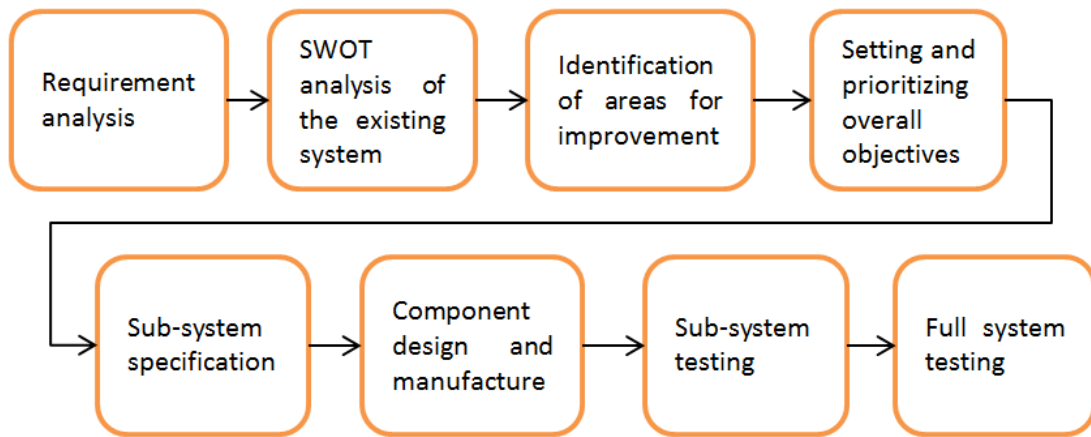





Figure 8. Approach to the development of the WMR 2013 robot.

3.1 Requirement Analysis

Table 3. USAR requirement analysis

Mobility	<ul style="list-style-type: none"> • Navigate complex terrain • Clear a standard door width of 72cm • In the competition piles of rubble are simulated by step fields, while ramps may represent collapsed wall or ceiling sections (Figure 9).
-----------------	--

	 <p>Figure 9. Step field and 45 degree ramp in a RoboCup Rescue competition.</p>
<p>Manipulation</p>	<ul style="list-style-type: none"> • Manipulate small items (e.g. a water bottle) • Access victims in narrow crevices at a maximum height of 1.6m (Figure 10 (a)) • Build structural shoring to support a column (Figure 10 (b)) <div style="display: flex; justify-content: space-around; align-items: center;"> <div data-bbox="477 1151 917 1581" style="text-align: center;">  <p>(a)</p> </div> <div data-bbox="971 1151 1273 1581" style="text-align: center;">  <p>(b)</p> </div> </div> <p>Figure 10. (a) WMR robot accessing a victim box in 2012 German Open. (b) The new structural shoring task (Pellenz 2013).</p>
<p>Power</p>	<ul style="list-style-type: none"> • Batteries must endure a 25 minute competition run
<p>Victim identification</p>	<ul style="list-style-type: none"> • Identify victims using: <ul style="list-style-type: none"> ○ Form ○ Visual – eye charts, hazmat labels, QR codes

	<ul style="list-style-type: none"> ○ Heat ○ Sound – two way audio ○ CO2 – to detect breath
Control	<ul style="list-style-type: none"> ● The robot must be autonomous, teleoperated by a single operator, or some combination thereof. ● Intuitive tele-operated controls. ● Operator station easy to set up by one person.
Mapping	<ul style="list-style-type: none"> ● Generate map of the site in GeoTIFF format ● Mark victim locations
Reliability	<ul style="list-style-type: none"> ● Real-world applications would require the robot to be both reliable and robust.

3.2 SWOT Analysis

Testing in the lab and during the Imagineering fair (The Imagineering Foundation 2012) was performed to develop a SWOT analysis of the existing system (Table 4).

Table 4. SWOT analysis of the existing system.

Strengths	Weaknesses
<ul style="list-style-type: none"> ● Highly mobile. Received best in class award in the 2012 European competition ● Strong and stable manipulator arm. ● Wide range of sensors. 	<ul style="list-style-type: none"> ● Arm uses joint control – takes practise. ● Poor graphical user-interface (GUI) layout. ● Head suffers from vibrations. ● Some devices fail to power up consistently while others are completely non-functional. ● Batteries are very difficult to connect/disconnect and no charge information is available.
Opportunities	Threats
<ul style="list-style-type: none"> ● The LiDAR and IMU devices could be used to implement mapping ● Inverse-kinematics control for the arm 	<ul style="list-style-type: none"> ● The poor state of the robot's wiring make it difficult to diagnose faults. ● The flipper motor brackets bend

<ul style="list-style-type: none"> • Remotec’s expertise and testing facilities could be used to improve the robot’s ruggedness. • Competing in the world competition may help to attract sponsors. 	<p>during normal use, suggesting a design flaw.</p> <ul style="list-style-type: none"> • The software is undocumented and contains a lot of unused code, so making changes is time-consuming.
---	--

It was found that the existing system had a large number of useful features in theory. Despite this the robot’s actual performance was poor, mainly due to low reliability and poor operator feedback. A number of expensive sensors had been purchased in previous years but some were not used at all, while others failed to live up to their potential.

3.3 WMR 2012/2013 Objectives

With the above in mind the objectives for the 2012/2013 team were set as follows.

Improve **reliability** of the system by:

- Increasing the strength of the chassis to withstand 0.5 m drops without permanent damage
- Reducing vibrations in the head
- Eliminating recurring failures in the electrical system

Improve operator **awareness and control** by:

- Using inverse kinematics to control the arm
- Designing a more intuitive control interface
- Providing feedback to the operator from all sensors

Progress towards real world **readiness** by:

- Carrying out a full system test in a realistic scenario
- Taking measures to proof the robot against the elements
- Redesigning the battery system for ease of use

4 Chassis

4.1 Initial State

The 2012 chassis was fabricated from steel sheet (Figure 11). Additional strength was provided by two aluminium brackets and a base-plate (Warwick Mobile Robotics 2012).

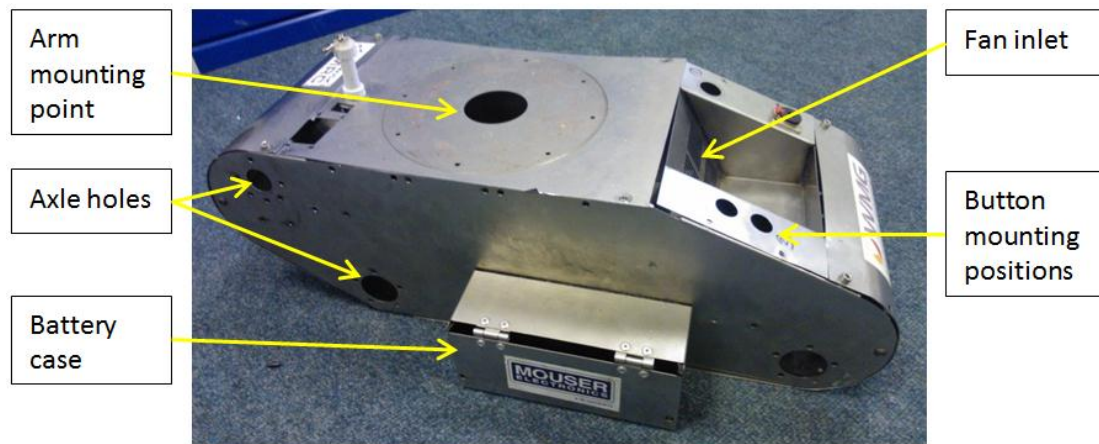


Figure 11. Old WMR chassis.

During initial testing a number of issues with the existing chassis were identified:

- Deformation due to operating loads leading to excessive vibrations and difficulty in driving the robot.
- Flipper motor brackets were damaged. This has been a recurring issue (Figure 12) due to the uncertainty of impact loads.
- Centre of mass of the robot was set high and towards the back requiring the robot to be driven in reverse up steep inclines.



Figure 12. Previous flipper bracket designs deformed.

4.2 Specification

1. Increase strength of the chassis to withstand 0.35 m drops without deformation whilst reducing weight.
2. Redesign flipper brackets to withstand service loads.
3. Reposition internal systems to move the centre of mass down and forward.

4.3 Chassis Redesign

4.3.1 Load Estimation

Initially, accurate estimates of the loads the robot must withstand during operation were obtained. For physical testing an inertial measurement unit (IMU) (Xsens Technologies B.V. 2013) was attached and the robot was driven from a step height of 0.35m (Figure 13). This was then simulated in SolidWorks (Figure 14) (detailed results in Appendix A.1).

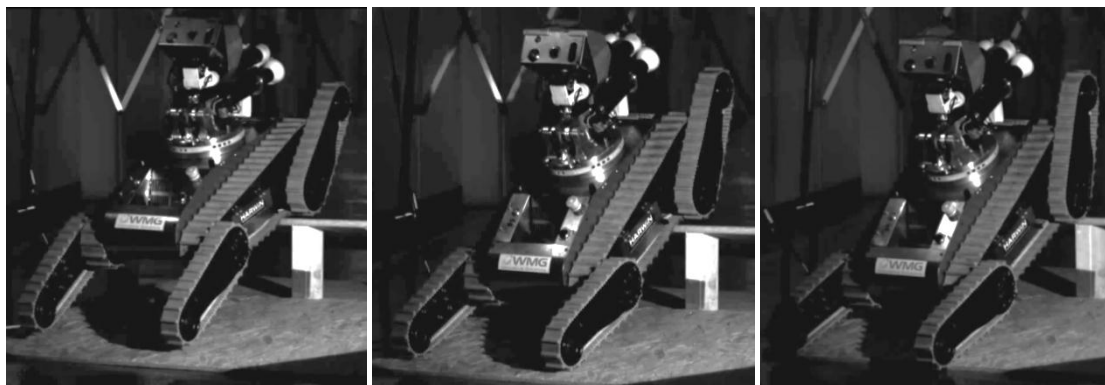


Figure 13. Time-lapse from high-speed footage of a drop test.

To validate the virtual test acceleration plots were compared and found to be similar with peaks of 41ms^{-2} for the physical test and 45ms^{-2} for the virtual test. This 9.75% error can be accounted for by SolidWorks' limitations such as the need to define contact points and the fact that bodies are treated as perfectly rigid (in fact some energy is absorbed in elastic deformation).

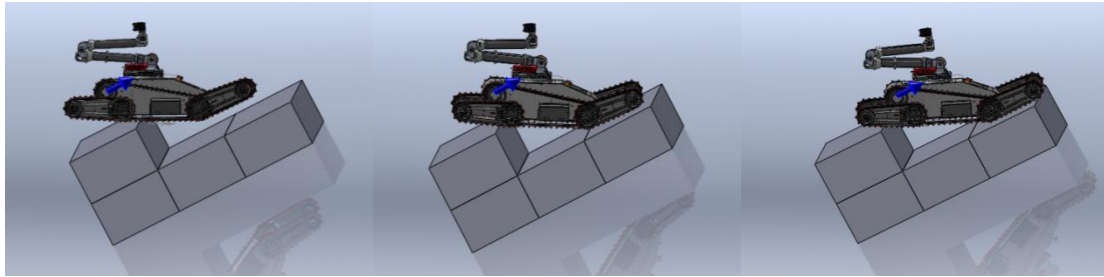


Figure 14. Time-lapse of a SolidWorks drop test.

A number of tests were carried out using the validated model. The results were used to calculate the forces experienced by flippers during impact (1520 N) and the force transmitted to the flipper motor bracket (18.2 kN). These values were used as loads for the new chassis design.

4.3.2 Space Frame Design Evolution

A structural space frame design was adopted for the new chassis. This provides a straightforward design for absorbing various impact loads. There are 6 key force transfer locations: two flipper shafts, two flipper motors and two drive motors. The initial design concept (Figure 15) shows the basic shape of the frame.

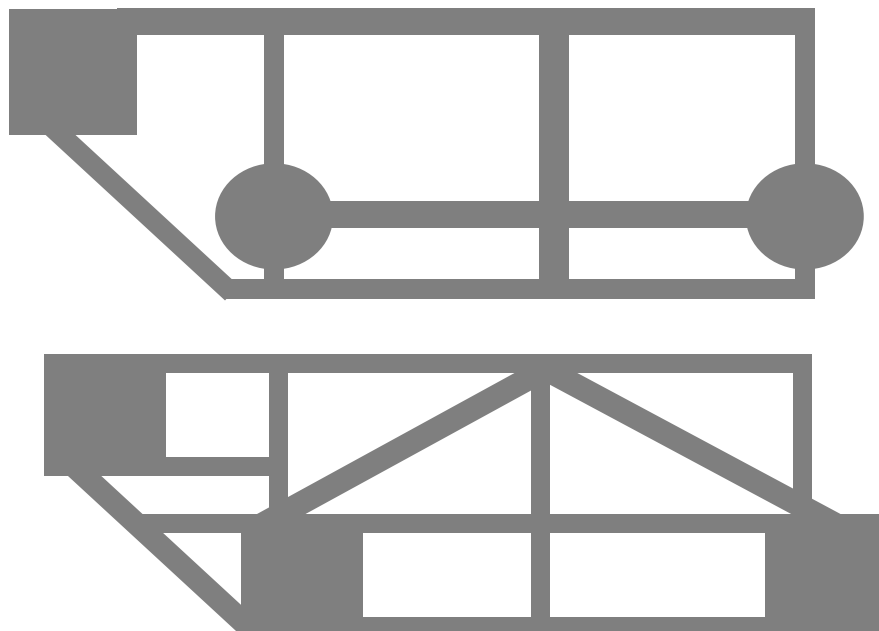


Figure 15. Sketches of the first chassis design concepts.

Aluminium alloy 6082-T6 was chosen as this provides high strength (310 MPa yield (alu Select 2013)) combined with low weight. 5 mm plate was used with cut-outs in non-critical areas to further reduce weight (Figure 16).

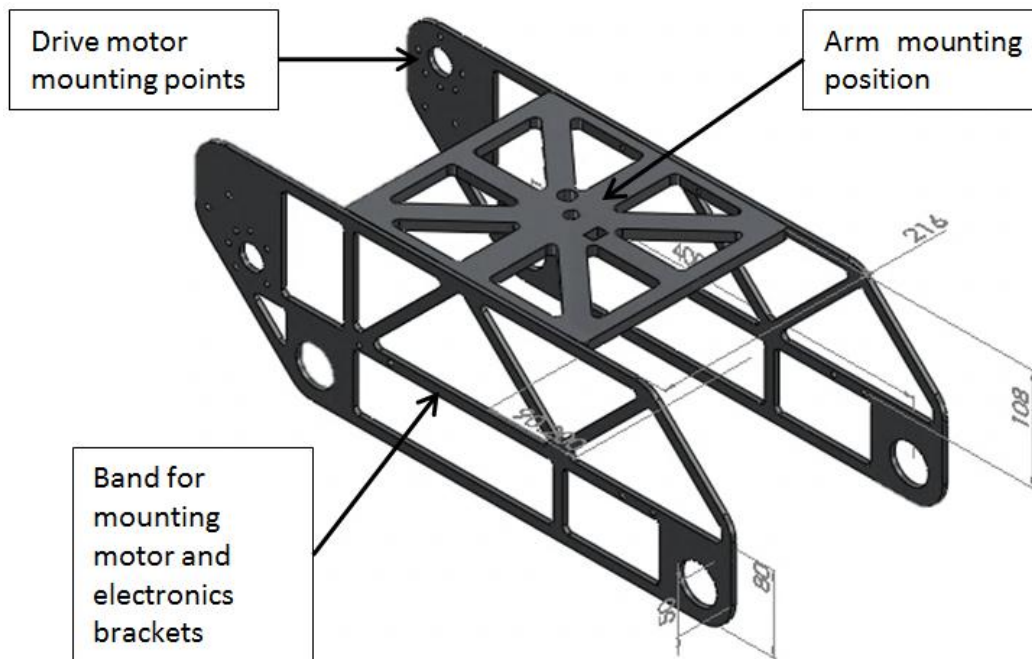


Figure 16. CAD drawing of an early design.

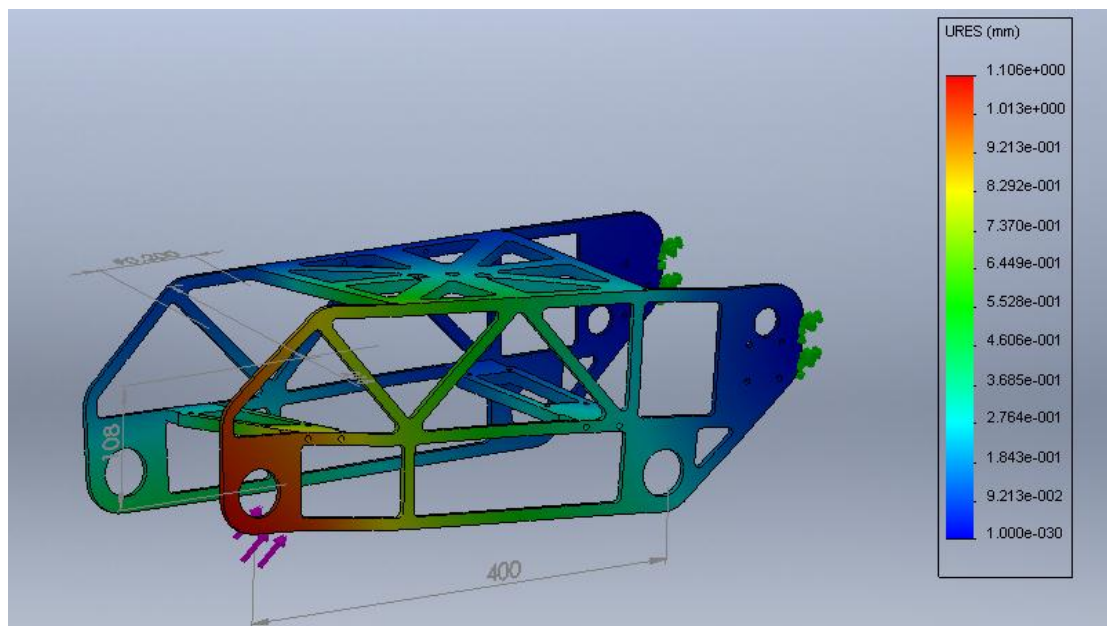


Figure 17. Preliminary frame FEA showing deformation under offset impact load.

By loading the space frame in various scenarios (Figure 17) (see Appendix A.2 for details) the design was refined by adding/removing material depending on stresses at particular points (Figure 18). The rounded edges at the front and back were added to provide a sliding guide to help negotiating steps. The thick band in the centre shares the forces generated by flippers during impact.

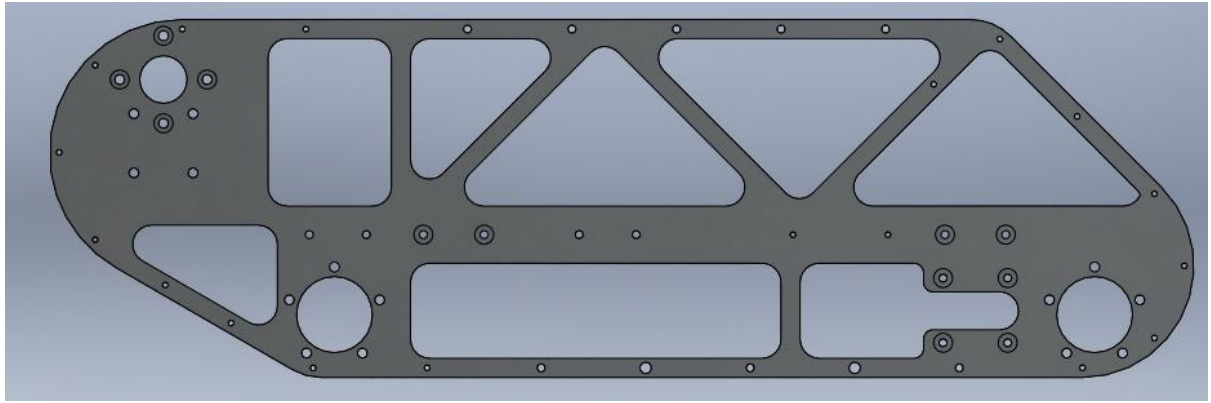


Figure 18. Final chassis side design.

4.3.3 Flipper Motor Brackets

4.3.3.1 Bending Force Estimation

Before redesigning the flipper motor brackets the forces involved in bending last year's designs were investigated (Figure 19).

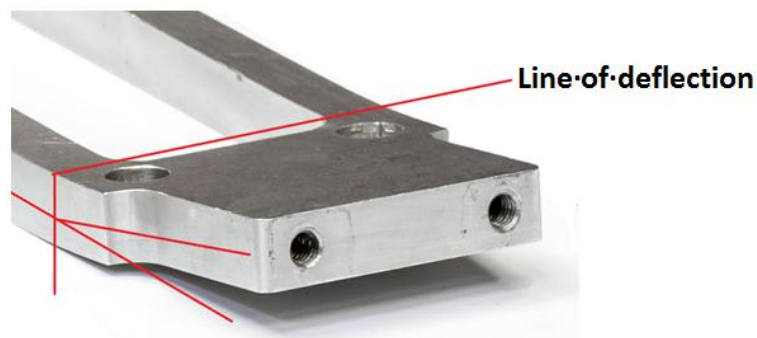


Figure 19. Deformation of 2012 flipper motor bracket.

The loading cases for the front and rear flipper motor brackets were different. The rear motor was mounted above the flipper shaft (Figure 20 (a)). This led to a reduced effective second moment of area of the bracket causing the stresses to exceed the yield stress of the aluminium alloy used (see Appendix A.3 for analysis). It was found that the forces to induce permanent deformation were 15.1 kN for the front bracket and 1.3 kN for the rear bracket. Moving the rear motor to a lower position (Figure 20 (b)) improved the loading condition and also brought the centre of mass forward and down.

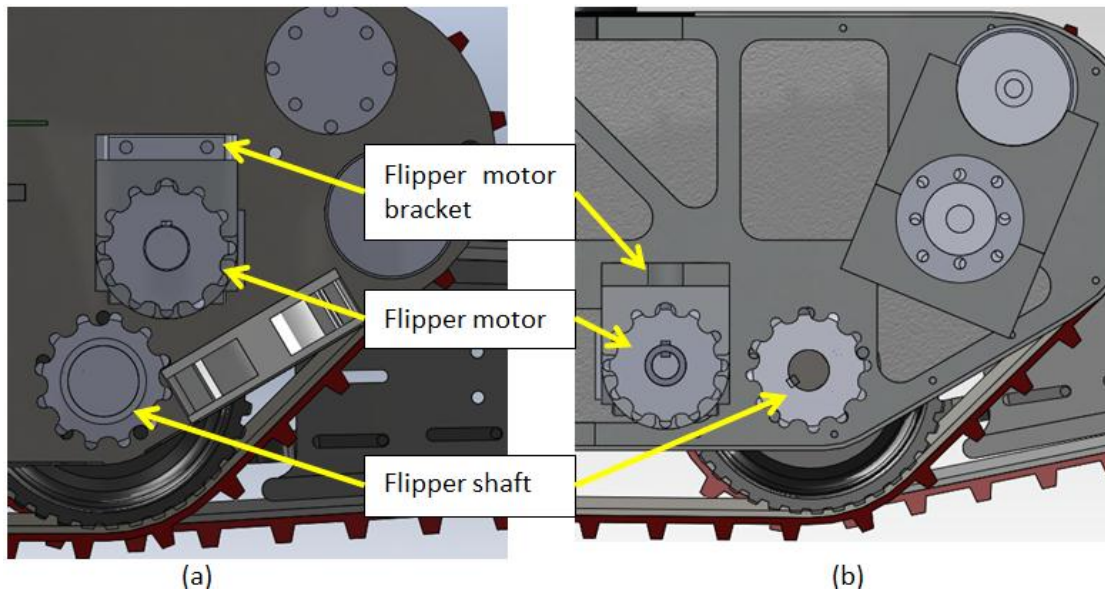


Figure 20. Position of the flipper motor in (a) 2012 design (above the flipper shaft) and (b) 2013 design (next to the flipper shaft).

4.3.3.2 Flipper Motor Bracket Design

Two major changes were implemented in the new flipper motor bracket design:

- Material was upgraded to aluminium alloy 6082-T6 (heat treated and artificially aged to increase yield strength).
- The outline of the part was redesigned to be much simpler and free of stress concentrations (Figure 21).

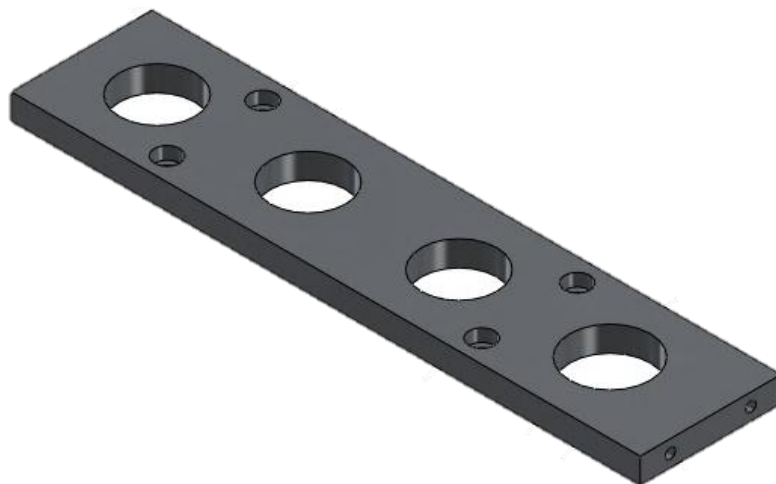


Figure 21. Redesigned flipper motor bracket.

A safety factor of 2 was applied in the design process. This means that the new parts can withstand loads up to 31.6 kN (see calculations below) without deformation:

$$I = \left[2 \times \left(\frac{0.01 \times 0.0125^3}{12} + (0.0125 \times 0.01 \times 0.02125^2) \right) \right]$$

$$I = 1.161 \times 10^{-7} m^4$$

$$W > \frac{310 \times 10^6 \times 1.161 \times 10^{-7} \times 0.25}{0.06 \times 0.19 \times 0.025}$$

$$W > 31.6 kN$$

4.3.3.3 Motor Shaft Support Bearing

It was recognized that providing a stronger motor mounting bracket could result in the impact loads bending the motor shaft. It was essentially unsupported (i.e. a cantilever). This was addressed by:

- Designing a silver steel shaft extension bush (Figure 22)
- Supporting it in a bearing capable of supporting flipper loads (up to 4.62 kN) (part number 61903-2rs1 (SKF 2013))

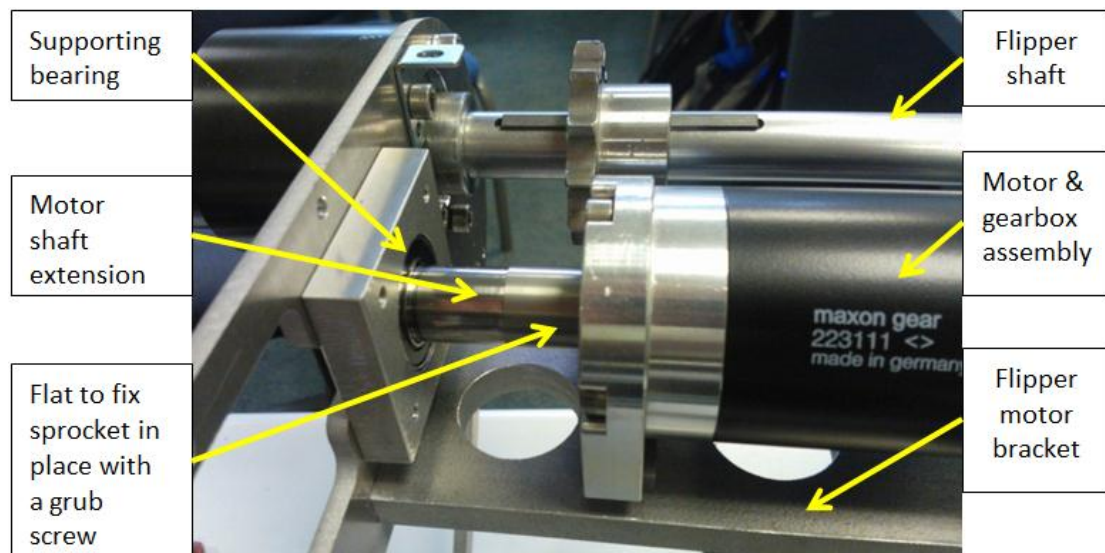


Figure 22. Motor shaft supporting bearing arrangement (view from the bottom).

4.3.4 Other Structural Components

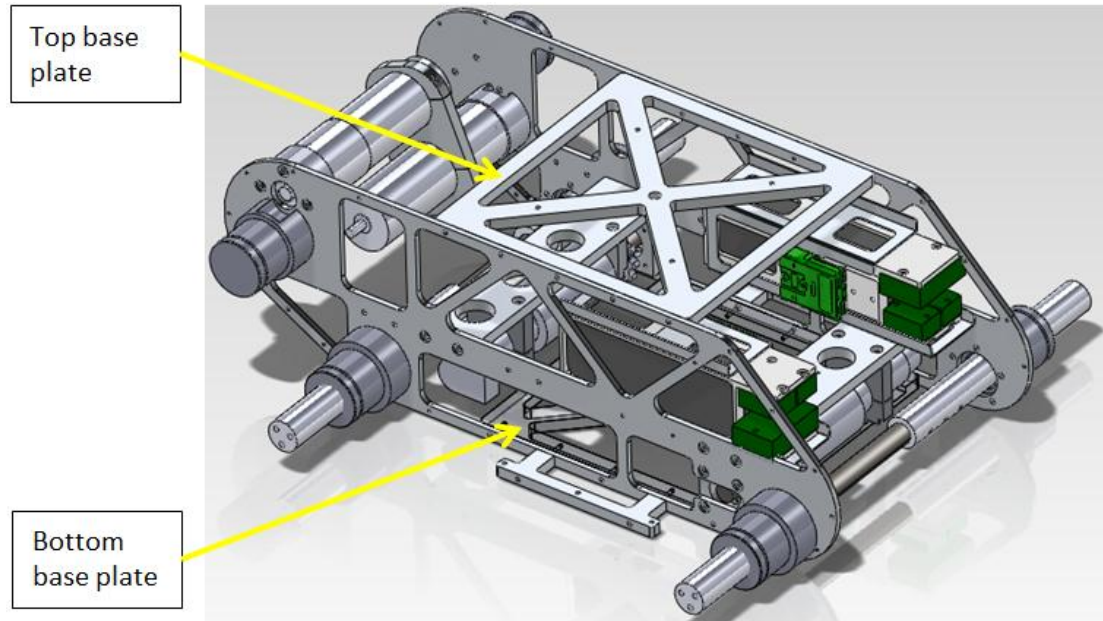
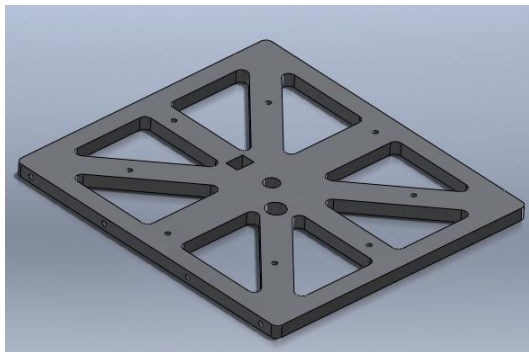


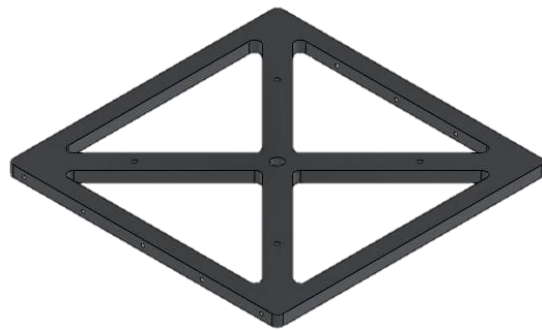
Figure 23. Space frame with additional components.

To complete the structure of the space frame (Figure 23) two supporting base plates were added. These were evolved from past designs (Figure 24):

- Material grade increased to 6082-T6
- Excess material was removed to save weight



2011 base plate



2013 base plate

Figure 24. Comparison of initial and redesigned base plates.

To increase the lateral stiffness at the rear of the chassis a bracket was added (Figure 25).

This ties together the drive motors and acts as cross-bracing.

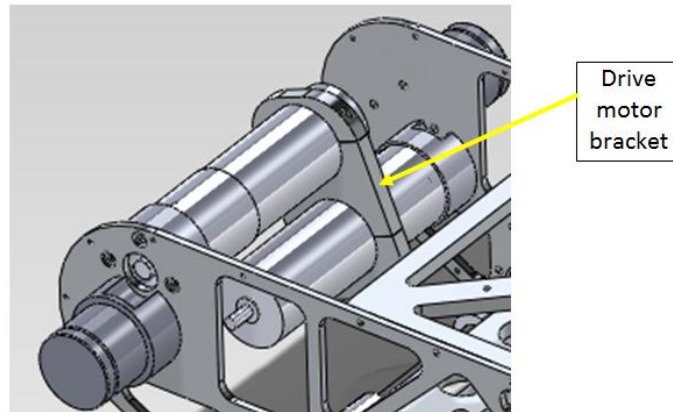


Figure 25. Drive motor bracket providing a cross-bracing effect at the back of the chassis.

4.3.5 Flipper Shafts

The flipper shafts had to be lengthened as the chassis had been widened. A split shaft design was adopted (Figure 26) for ease of assembly and maintenance. Location was provided by a set of grub screws resting on a flat on the central part of the shaft.

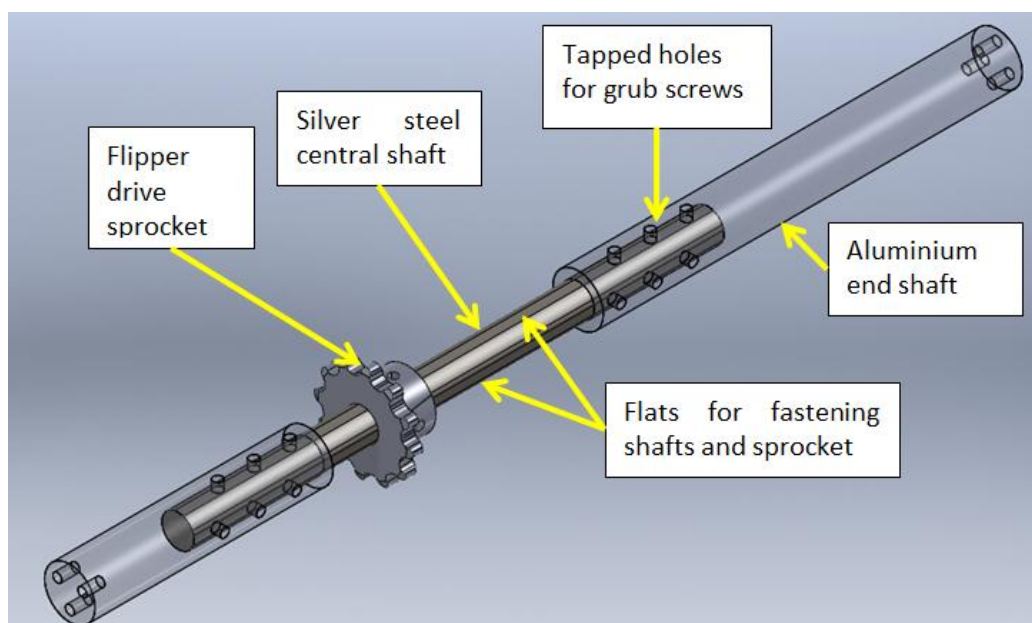


Figure 26. New flipper shaft design.

4.3.6 Internal Layout

The aim of rearranging the internal layout of the robot was to bring the centre of mass forward and down while maintaining access to critical components. Due to the fact that CAD data was not available for off-the-shelf components a cardboard model was constructed (Figure 27) to investigate various layout options.

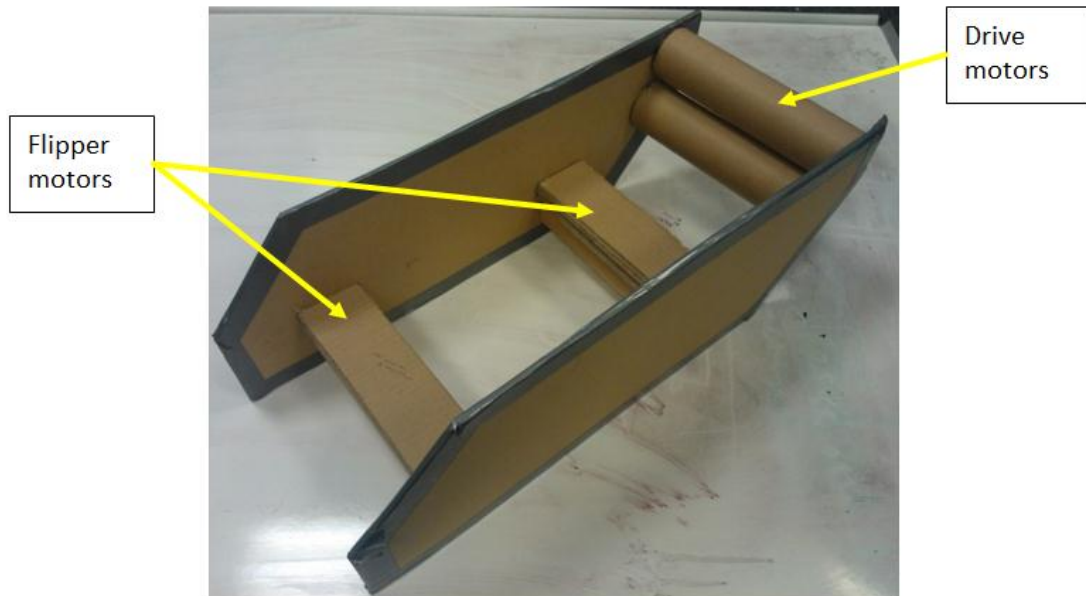


Figure 27. Cardboard model used to investigate internal layout options.

In order to minimize the weight of the head and increase the weather-proofing of the robot a number of components were moved into the chassis. The width of the chassis was increased by 24 mm to accommodate the components (Figure 28) with enough wiring space.

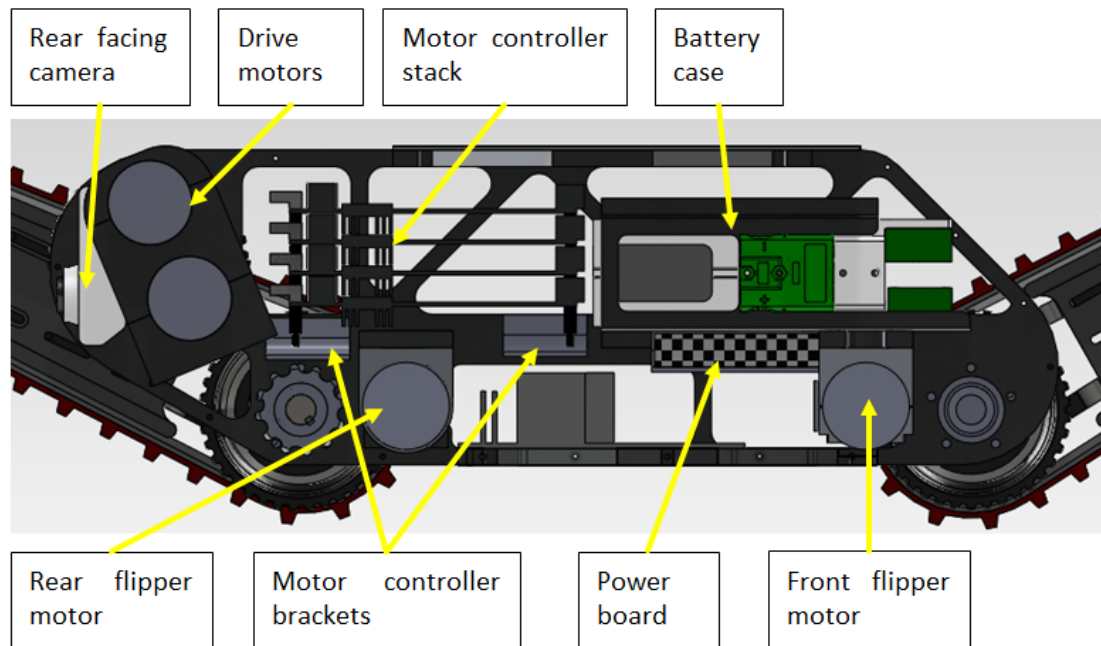


Figure 28. Final internal layout.

4.3.6.1 Thermal Modelling

It was intended to provide no vents in the shell covering the chassis in order to prevent the ingress of dust and water. However, electronic components still required cooling. This can be done by circulating air within the chassis to move heat from the hot components to the

large thermal mass of the chassis. In order to determine the optimum airflow for cooling and the number and placement of fans SolidWorks flow simulation was used (see Appendix A.4 for details).

A worst case scenario was assumed where drive motors are at full power. It was found (Figure 29 and Figure 30) that sufficient cooling is achieved by having two small fans blowing air over motor controller heatsinks and a third large fan forcing air movement throughout the rest of the chassis (Figure 31). This ensures an even temperature distribution in the steady-state without any of the components overheating.

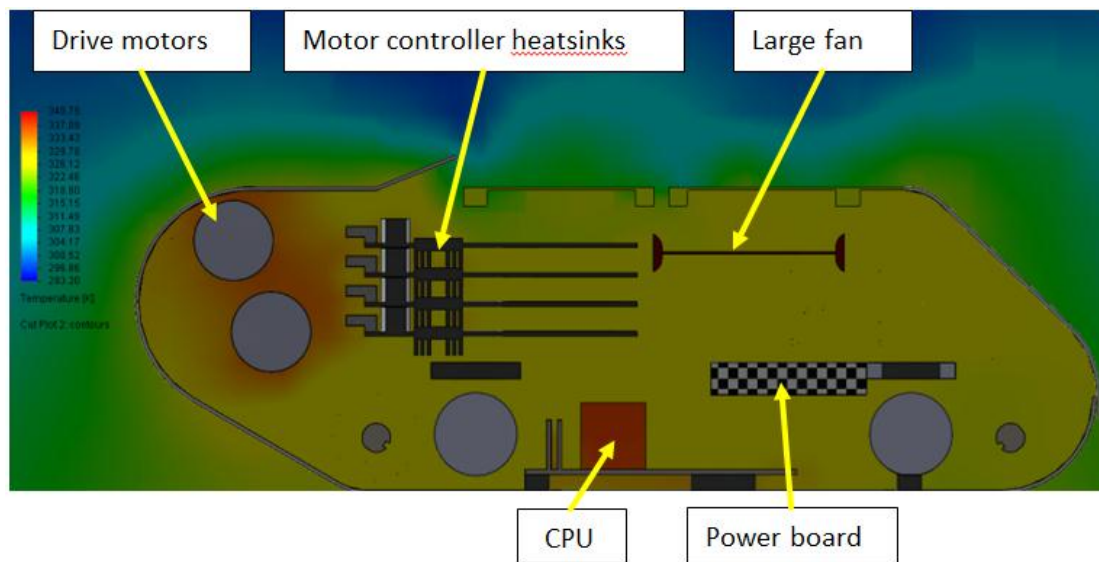


Figure 29. Temperature distribution in the robot (one large and two small fans). Side view.

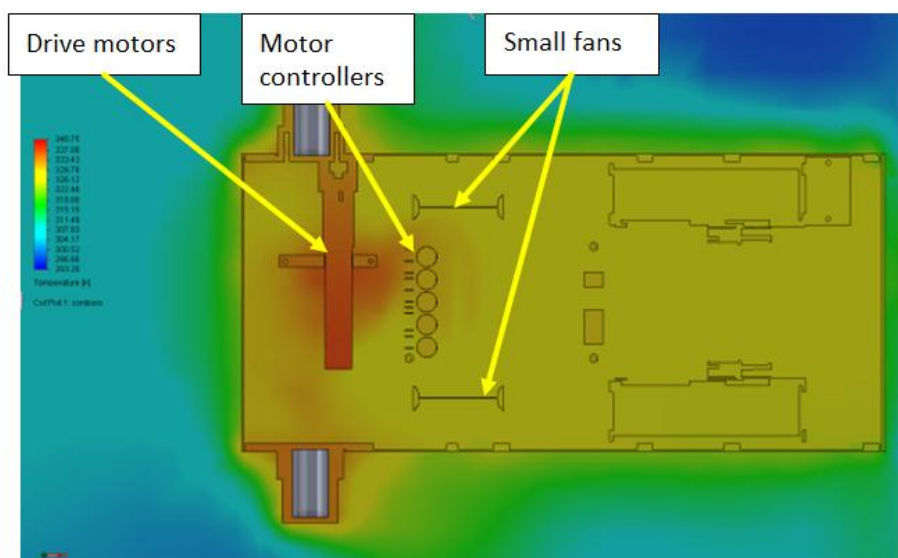


Figure 30. Temperature distribution in the robot (one large fan and two small fans). Top view.

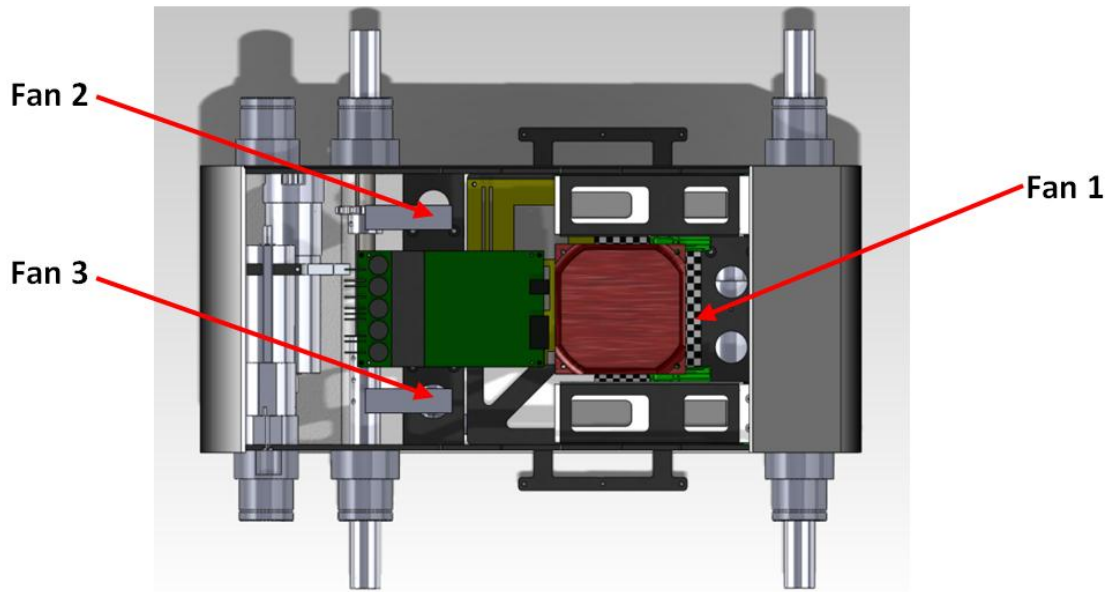


Figure 31. Final arrangement of fans.

4.4 Shell Design

To cover the newly developed chassis a new non-structural shell was designed. It functions as a barrier to dirt and moisture and removal provides access to components inside the robot. It does not have to carry any significant loads as these are supported by the chassis. The material chosen was ABS (see Appendix A.5).

4.4.1 Panel Design

The stresses induced shell panels were modelled using beam bending theory (see Appendix A.6 for details). Thickness of 3 mm was chosen as a result (safety factor of 1.97).

The actual panel geometry is a trade-off between the protection of internal components, accessibility and ease of manufacture (Figure 32 and Figure 33).

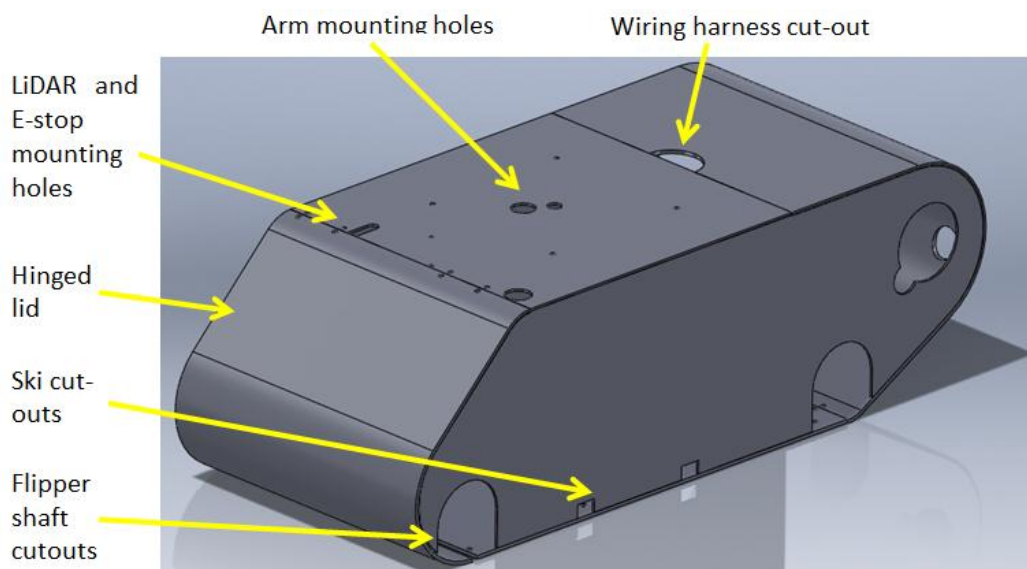


Figure 32. Final shell design with cut-outs.

The seams at the bottom of the shell (Figure 33) can be sealed with a silicon compound if the robot is to be operated outdoors.

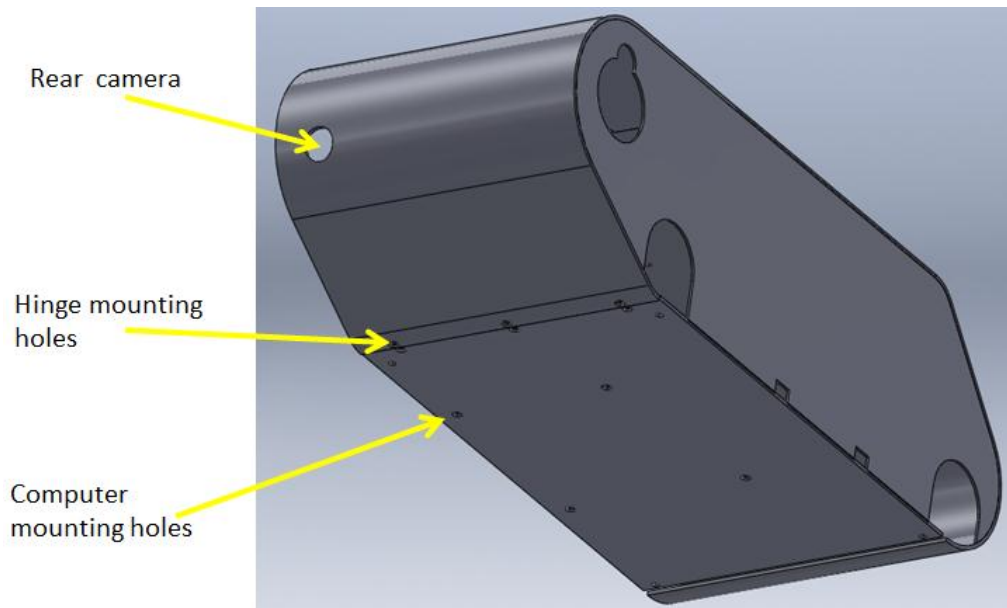


Figure 33. Final shell design with cut-outs (bottom view).

4.5 Results

- Chassis strength increased eliminating deformation during service
- Weight decreased by 23%. This extends battery life
- Centre of gravity moved forward and down improving slope climbing capability
- No permanent deformation of redesigned flipper brackets observed during testing
- Better protection from the elements by eliminating air intakes and locating batteries internally

5 Power System

5.1 Introduction

The power system comprises batteries, regulators, switches, fuses, connectors and wiring.

The focus was on improving:

- Battery enclosure, where the batteries are located within the robot and connected to the power system.
- Battery management system, which ensures that the batteries' safe operating limits are not exceeded and provides information about the batteries to the CPU.
- Power distribution board, which regulates the battery voltage and supplies power to the electronics.
- Internal wiring, carrying power and data throughout the robot.

5.2 Battery Enclosure

5.2.1 Issues Identified

1. While attending the Imagineering fair (Ricoh arena, 20th-21st Oct 2012) it was noted that the robot's flippers could obstruct access to the battery enclosures. If emergency stopped, it would be very time-consuming to remove the batteries, posing a safety hazard.
2. The enclosure had several sharp edges (a safety hazard) (Figure 34).
3. The batteries' power connectors were awkwardly positioned. As a result, replacing the batteries could take several minutes.
4. The modular nature of the connector meant that the battery could be connected with the wrong polarity.

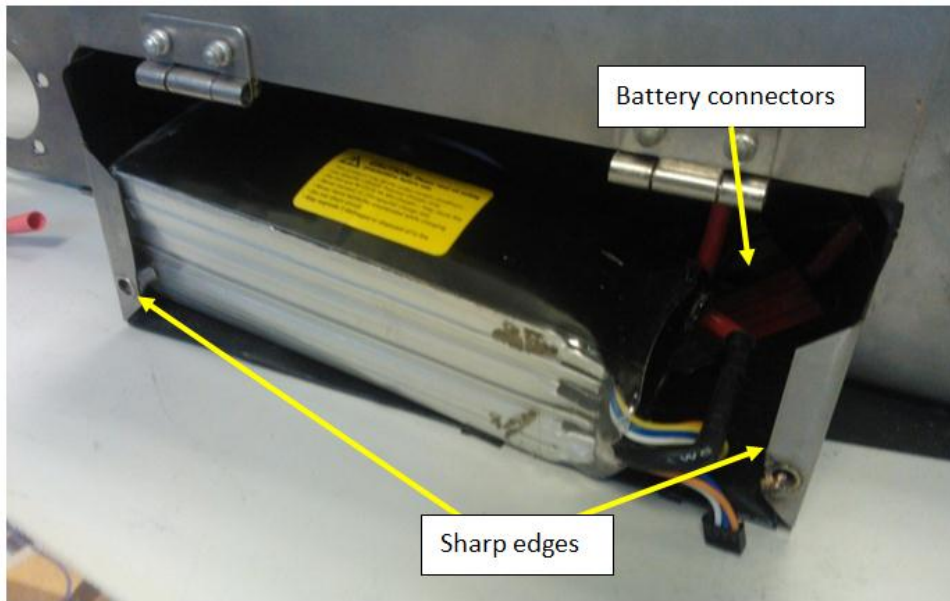


Figure 34: Photo of the original battery enclosure

5.2.2 Specification

1. Batteries must be located where they are easily accessible at all times.
2. The enclosure must be free of sharp edges which would pose a risk to wires or the operator during connection and disconnection of the battery.
3. Replacing the batteries must take less than a minute.
4. It must be impossible to connect the batteries with reverse-polarity.

5.2.3 Actions

Due to the internal layout of the robot it is back heavy. Therefore, locating the batteries under the front lid is advantageous as it moves the centre of mass forward. Furthermore, the front of the robot can be opened easily to allow access to power board connections, computer ports (for debugging purposes) and on/off buttons.

The battery connector should be asymmetric (i.e. connectable only the correct way) and rated above 24V and 60A. Additionally, data pins are required to transmit data from the battery management system to the power board over I²C bus. APP SBS75X (Figure 35) (Anderson Power Products 2012) was chosen as it has been proven as reliable and fits the specification.

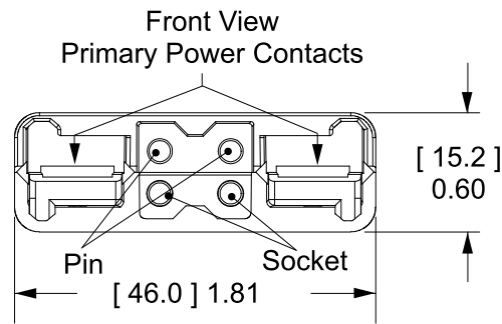


Figure 35. APP SBS75X connector rated at 80V, 110A. Dimensions in [] in mm (Anderson Power Products 2012). The mating/unmating force of the connector is 70N. This was used as a design load to optimize the form and size of the battery case and holder. The former was fabricated from sheet aluminium while the latter was 3D printed in ABS (Figure 36).

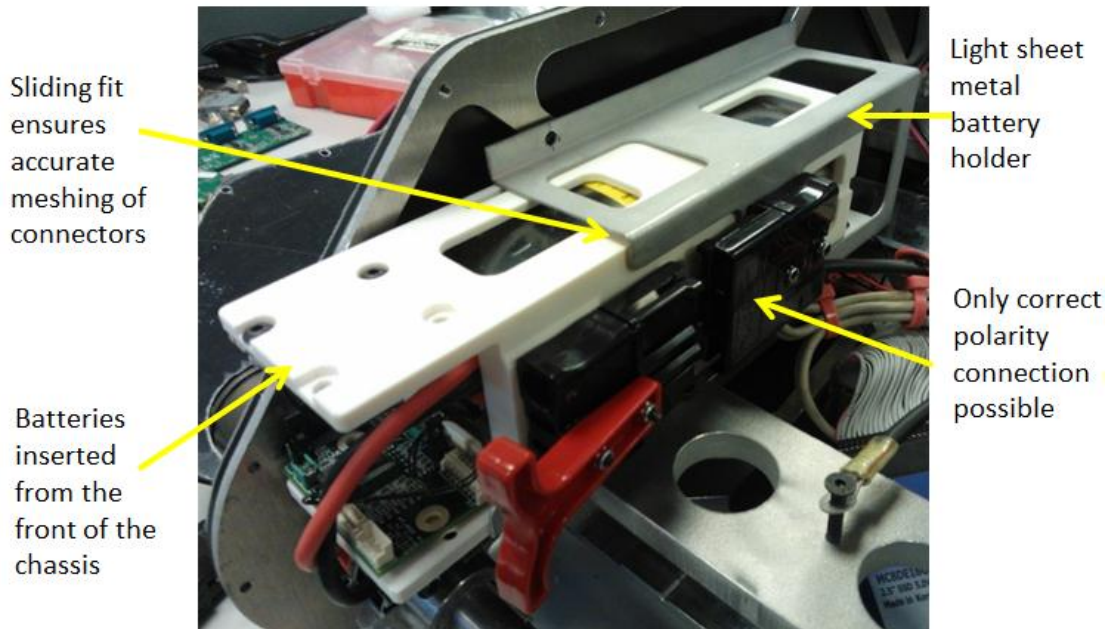


Figure 36. Redesigned battery-pack and holder.

The manufactured battery cases (Figure 37) are sturdy and easy to insert and remove from the robot. This is especially important in case of emergencies where a short-circuited or damaged battery must be removed from the robot quickly. Guiding rails were also added to the 3D printed part to ensure the connectors are always aligned accurately.

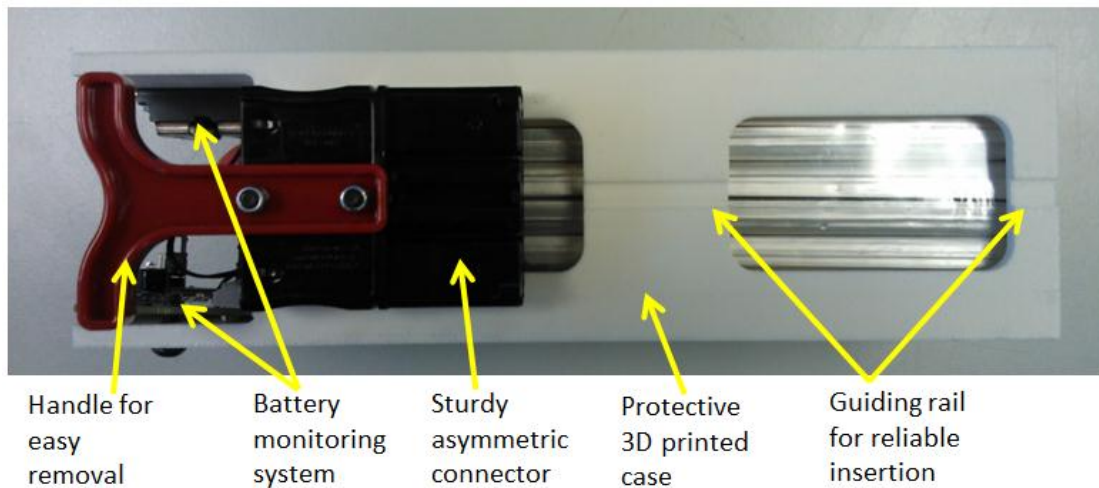


Figure 37. Redesigned battery-pack.

5.2.4 Results

1. The batteries are now easily accessible and cannot be obstructed by the flippers.
2. The battery is protected from sharp edges within the housing, and there are no sharp edges around the handle.
3. Replacing a single battery takes between 10 and 20 seconds.
4. Batteries cannot be connected with reverse-polarity

5.3 Battery Monitoring

5.3.1 Issues identified

1. The only fault-condition monitored was cell under-voltage. Short-circuits and other faults were not protected against.
2. In the event of a fault the battery had to be manually disconnected to prevent the battery being discharged further (with potentially catastrophic consequences).
3. No fuel-gauging was implemented.



Figure 38: Photo of the original battery monitor

5.3.2 Specification

1. The battery monitor must protect the batteries against cell undervoltage and short-circuit/overcurrent conditions.
2. In the event of an undervoltage or overcurrent condition, the battery monitor must automatically disconnect the battery.
3. The battery monitor must supply state-of-charge information to the robot's control system.

5.3.3 Actions

- A battery monitoring board was designed (Figure 39) using two ICs – one for protection, the other for fuel-gauging.
- The cell-voltage connectors were chosen to be compatible with the existing battery and charger connectors.

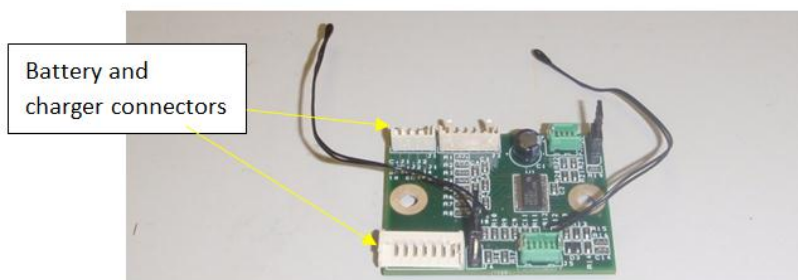


Figure 39: Photo of the new battery monitor

5.3.4 Results

1. The BQ77910A (Texas Instruments 2012) provides protection against under-voltage, excessive discharge current and short-circuit conditions. It can also protect against over-voltage and excessive charge current but this would interfere with the regenerative-braking provided by the AX3500 motor controllers (Roboteq 2013) and so was disabled.
2. Should a fault occur, the chip automatically switches an attached NFET off to prevent the battery discharging further. Recovery is automatic once the fault condition is removed.
3. The BQ34Z100 (Texas Instruments 2013) provides fuel-gauging reported to be accurate to less than 1% of capacity.

5.4 Power Board

5.4.1 Issues Identified

1. The 30W DC/DC converters used on the power board were not capable of powering all systems at full load. This would cause devices to stop functioning as their power supply cut out.
2. The output connectors (Figure 40) were not arranged in any obvious pattern. Adjacent connectors had different voltages and polarities, which was confusing when connecting devices.



Figure 40: Photo of the original power board

5.4.2 Specification

1. Each power supply must be able to power all devices of the supply's voltage at full load.
2. Connectors must be grouped according to voltage, with consistent polarity. Both voltage and polarity must be marked on the board.

5.4.3 Actions

- 50W DC/DC converters with heat-sinks were used to improve reliability and operating temperature range.
- Small footprint power-FETs reduced the size of the power switching section of the board.
- An mbed microcontroller (mbed 2013) was used to control the board since the supporting toolset made programming very straightforward.
- The pluggable screw-terminals were replaced with Harwin 101-Lok power connectors for higher reliability and current capacity.
- A 4-port I2C interface was added to allow the power board to communicate with the battery fuel-gauge chips.

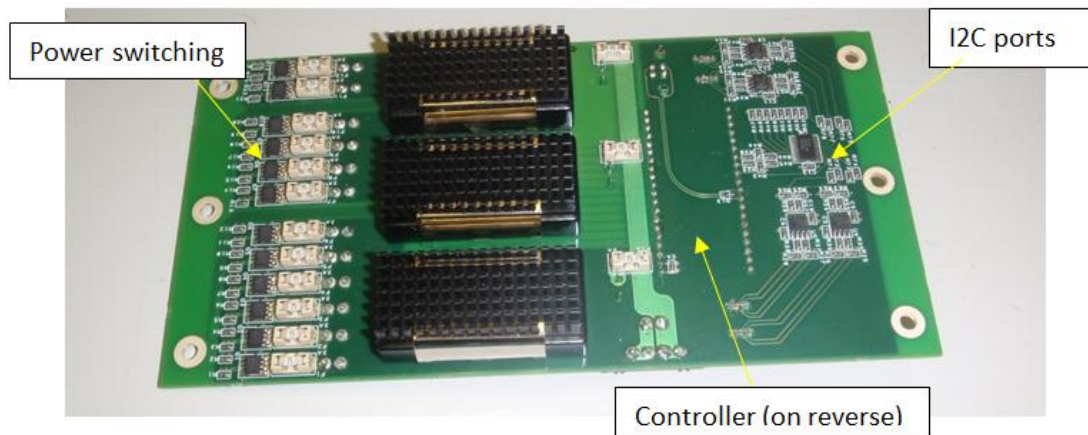


Figure 41: Photo of the new power board

5.4.4 Results

1. The new power supplies can source the maximum rated current for all attached devices with 20% spare capacity.
2. Connectors are grouped by voltage, with polarity labelled. Connectors cannot be connected with reverse-polarity.

5.5 Wiring

5.5.1 Issues Identified

1. There was no wiring diagram for the robot, which made maintenance more time consuming as connections had to be written down as they were disconnected to ensure that the device could be reconnected later.
2. The drive and flipper motors' power supplies were arranged in a large loop around the base of the chassis, effectively creating a loop antenna (Figure 42). This was a major concern as it could potentially interfere with not only the robot's electronics but also any nearby electronics.

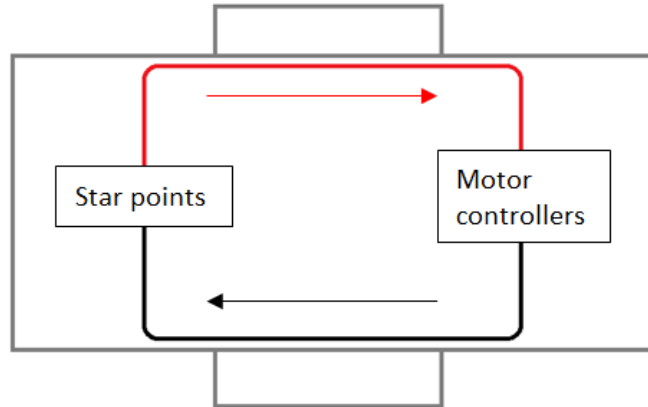


Figure 42: Original motor power supply wiring

5.5.2 Specification

1. A wiring diagram must be compiled, detailing all electronic systems within the robot, their ports and all wires, cables and connectors used to connect them.
2. Systems should be wired so that the current loop produced by their power supply (traced from either battery's positive terminal to its negative terminal) is as small as possible.

5.5.3 Actions

- A bus-bar was used to simplify power connections.
- The motor controllers were repositioned and rewired to eliminate current loops.
- All connections were noted and used to construct a wiring diagram for future reference (see Appendix B.1).

5.5.4 Results

1. A wiring diagram now exists detailing all connections between systems, including connector type, pinout and wire colours.
2. Current loops have been minimised.

6 Sensors and Devices

For the robot to perform its search and rescue tasks, various sensors and devices are mounted on the chassis and head. This section outlines the initial state of the robots capabilities followed by the team’s developments to improve the robot’s functionality.

6.1 Initial State

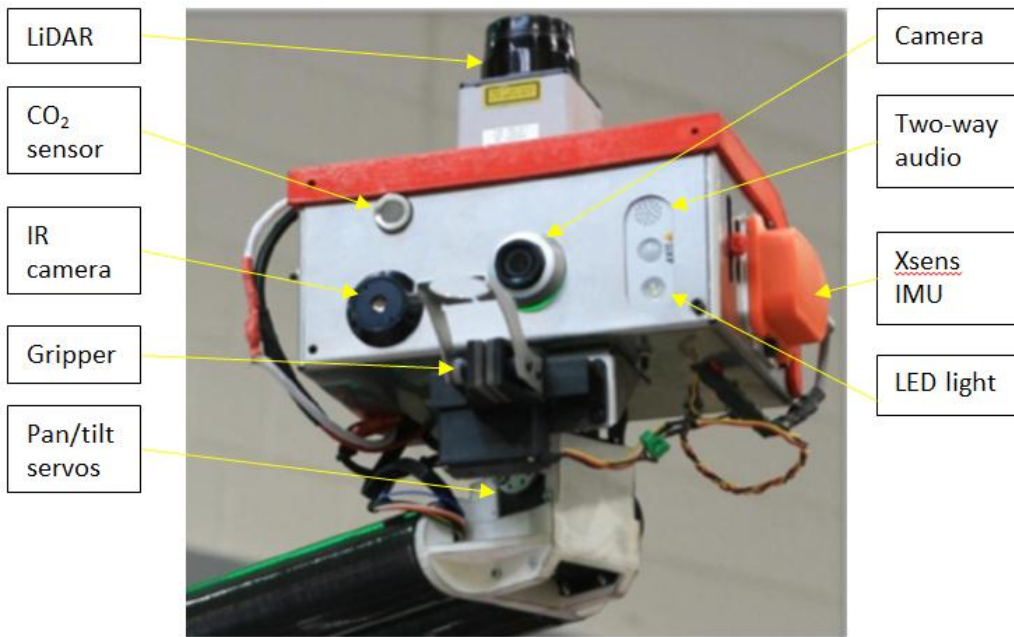


Figure 43. WMR 2012 robot head.

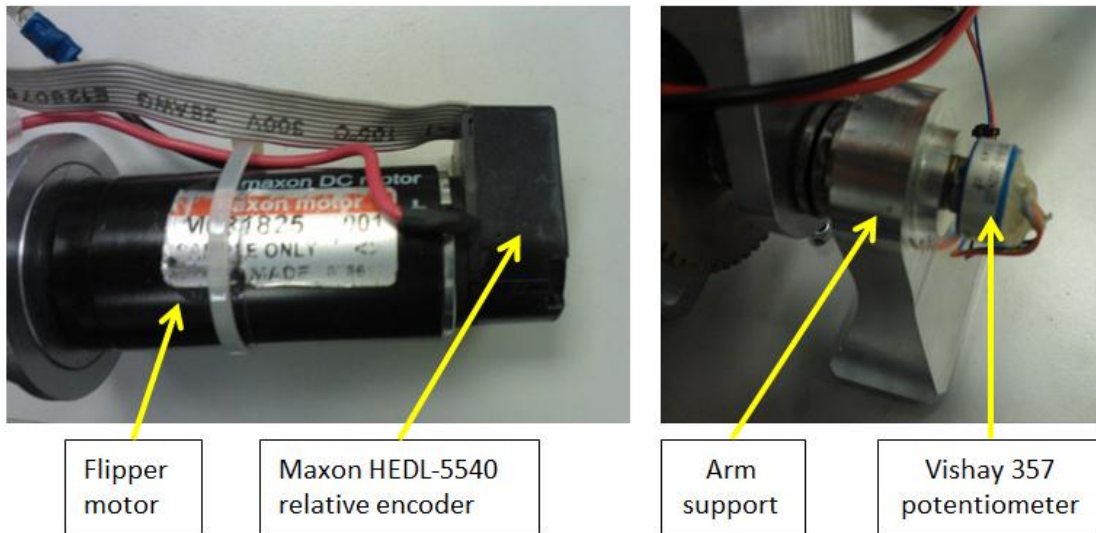


Figure 44. Existing position measurement sensors (a) on flipper motors, (b) on arm joints.

Sensors and devices were mounted both on the head of the robot (Figure 43) and within the body (Figure 44).

After initial testing, the capabilities of the robot were reviewed in terms of the devices/sensors used. Table 16 in Appendix C.1 shows the expected capabilities of the robot with the current devices/sensors that provide this capability and the strengths/weaknesses of this device in achieving this capability.

From the preliminary analysis, it was clear that in order to increase operator awareness an accurate portrayal of the flipper positions was necessary. The current encoders were relative and so could not be used to store the current flipper positions.

There were several sensors and devices that were attached to the robot but were either not working or had no function. These include:

- Gripper module
- Infrared camera
- IMU
- LiDAR

Initial testing showed that each of these devices were either unpowered or had no method of communication with the client; they were all however in working condition when tested separately from the robot.

6.1.1 Initial Head State

A SWOT analysis was performed on the previous head design (Table 5).

Table 5. Head design SWOT analysis.

<p>Strengths:</p> <ul style="list-style-type: none"> ● Holds all components ● Easy access to components from removable lid ● The design is strong and impact resistant ● Positioning of components in the head is ideal for unobstructed views 	<p>Weaknesses:</p> <ul style="list-style-type: none"> ● Camera, LiDAR and IMU exposed to the environment ● Cluttered by chaotic and unplanned wiring – makes it hard to access and remove individual components ● The design is wide and deep. This inhibits the amount the head can turn and tilt. ● The design is heavy and contains unused components - creates extra vibrations. ● Components are held in place by makeshift brackets and can move about
<p>Opportunities:</p> <ul style="list-style-type: none"> ● Make design more modular with specific areas for each component ● 3D printing knowledge in the group – using this technology would allow for more complicated internal design ● LiDAR and IMU are currently unused so could be removed/moved 	<p>Threats:</p> <ul style="list-style-type: none"> ● Could lose functionality if removing components ● If components are removed, more wires will need to run up the arm

The initial head design using sheet aluminium and a rapid prototyped cover had to be improved due to its weight and chaotic internal layout. The power distribution within the head was haphazard, illogical and confusing. This could explain some of the intermittent dropout problems that were occurring. A complete overhaul of the wiring needed to be completed.

The LiDAR and IMU were both previously in the head (increasing weight) yet non-functional, therefore a decision process was needed to decide whether or not these components should be kept in the head, moved elsewhere or removed completely (Table 6).

Table 6. LiDAR and IMU placement decision table

Keeping LiDAR and IMU in head	Moving LiDAR and IMU to body
<ul style="list-style-type: none"> • LiDAR does not have obstacles in front of it, such as flippers • Can use rotation of head for 3D mapping – would need extra gimbal if on the body 	<ul style="list-style-type: none"> • Reduced weight in the head • Less wiring to run up the arm and simplified wiring in the head • IMU data can give accurate and useful body orientation rather than head orientation • Can give useful 2D point cloud data, would possibly be too much vibration on head

The result of this process was the decision to remove the LiDAR and IMU from the head and place them on/ into the body. The other sensors were all kept in the head, but some electronic components were moved into the body to once again save weight.

6.2 Specification

To improve the robot beyond its current capabilities the following aims were set:

- Make all sensors work and communicate correctly with the GUI.
- Improve drivability and operator awareness through better use of the LiDAR, IMU, flipper encoders and potentiometers.
- Redesign of head unit to reduce weight and improve sensor layout.
- Reorganise wiring and layout to ensure all sensors and devices work correctly.

6.3 Actions

6.3.1 Implementation of Existing Devices

The LiDAR has been moved from the top of the head to the front of the body. It can be used with a SLAM algorithm to create a 2-D map of the surrounding environment; giving the

operator a clear view of their surroundings. This year, the LiDAR was predominantly used to provide information on what is directly in front of the robot to aid short-range navigation.

The IMU has been moved inside the body of the robot for orientation data, centre of mass calculations and stabilization of the LiDAR 2-D map. The calculation of the centre of mass, as well as diagrammatic display of the robot orientation aid the operator to recognize and take action if the robot is about to 'topple' over.

The gripper has been mounted below the head and supplied with PWM control. An mbed microcontroller was introduced to the head to supply the robot with the required PWM control.

The infrared camera has been implemented, providing data to the robot and the power issues have been solved by rewiring the head.

6.3.2 Sensor/ Device Changes

6.3.2.1 *CO₂ Sensor*

The CO₂ sensor circuit board was redesigned to ensure correct driving voltage is supplied. The circuit design is shown in Figure 45 (board layout in Figure 46). An operational amplifier is used to amplify the small change in voltage output from the sensor to be sent to the mbed microcontroller. A voltage regulator steps down the incoming 15 V to 6 V for the sensor, the capacitor values are calculated from the data sheet. The capacitor C3 is a decoupling capacitor.

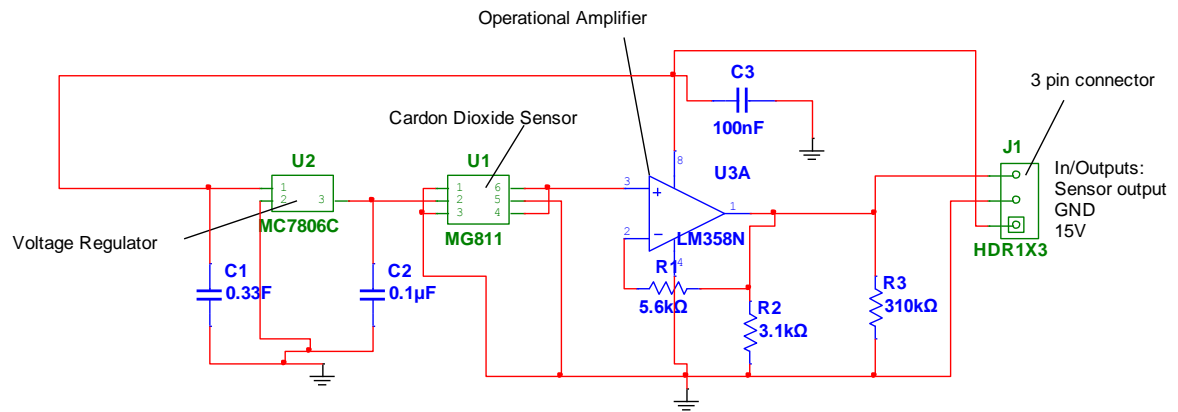


Figure 45. Circuit for CO₂ sensor.

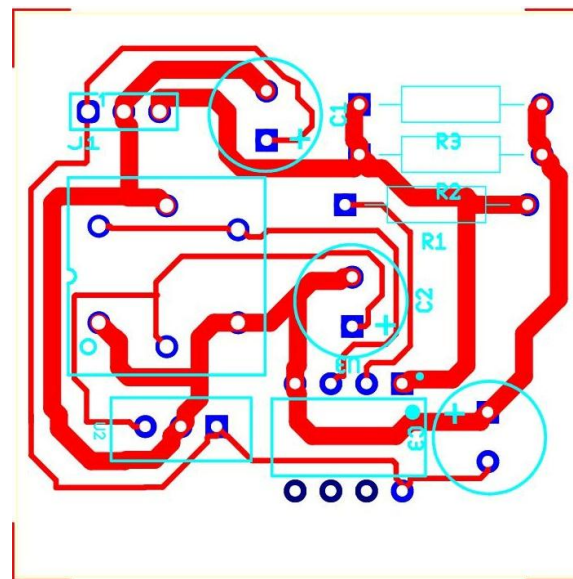


Figure 46. Ultiboard layout for CO₂ sensor board.

6.3.2.2 Flipper Encoders

Design of a system of absolute encoders to monitor the position of the robot's flippers was carried out by previous year's team (Warwick Mobile Robotics 2012). As the correct parts were already identified, it was decided to implement this system. For the flipper encoders to correctly operate two Melexis 90316KDC Hall-effect encoders were mounted on circuit boards and small magnets were attached to flipper motor shafts (Figure 47). The boards were connected to the flipper motor controllers to provide absolute position feedback.

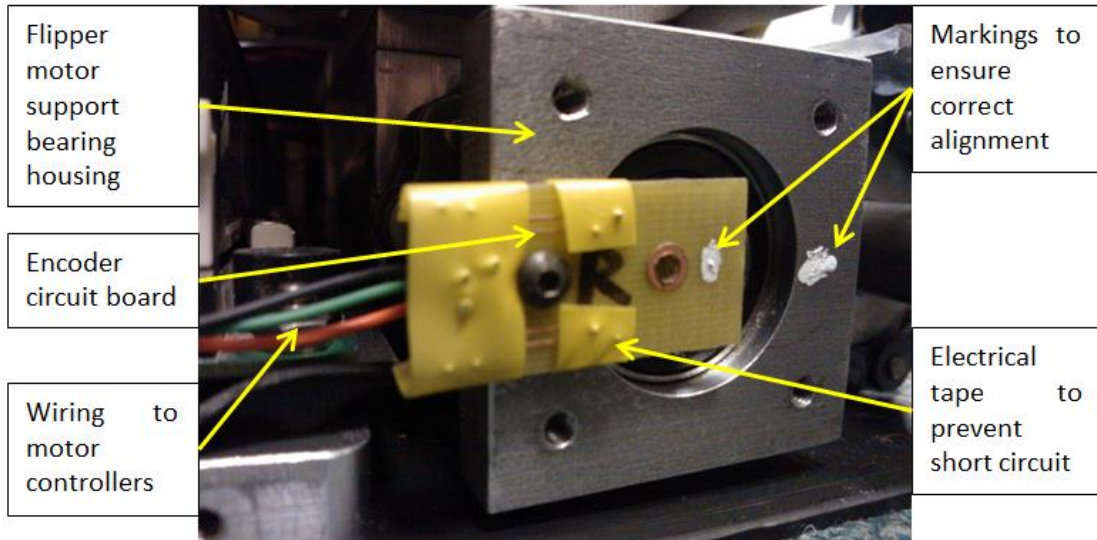


Figure 47. Encoder circuit mounted on flipper motor bearing housing.

6.3.2.3 mbed Microcontroller

For the CO₂ sensor and gripper module to communicate to the central computer an ARM mbed microcontroller (mbed 2013) was introduced into the head. This is required to:

- convert the analogue CO₂ sensor data to digital data and send it to the computer
- receive gripper target position from the computer and supply the correct PWM control signal to the gripper

Figure 48 shows the circuit of the mbed (board layout in Figure 49). The two resistors are to drop the high voltage coming in from the CO₂ sensor to a voltage suitable to input to the mbed.

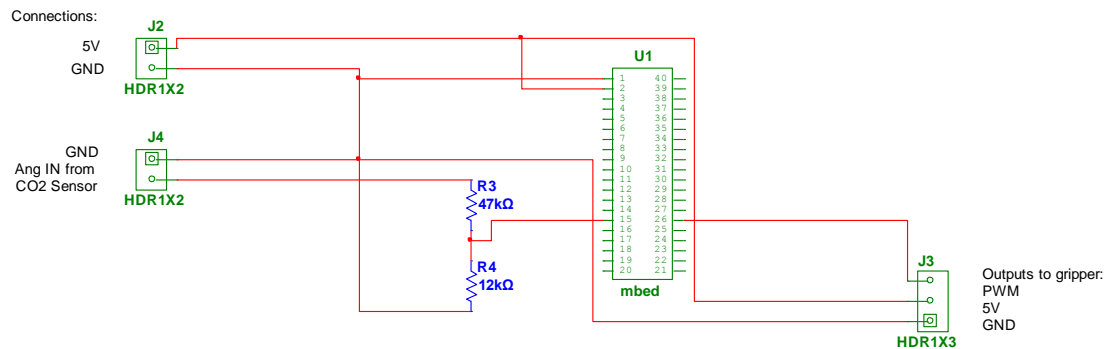


Figure 48. Circuit layout from mbed board.

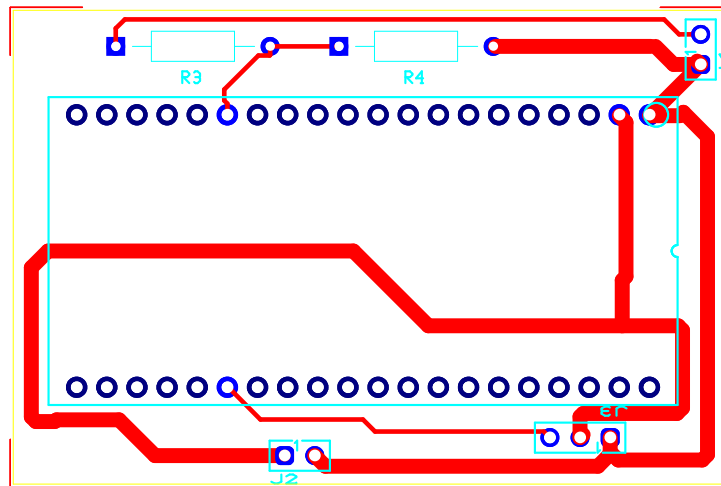


Figure 49. Ultiboard layout for the mbed board.

6.3.3 Head Redesign

6.3.3.1 Design Specification for the New Head

- Reduced weight
- Reduced size
- Must fit and protect all components within
- Organised layout, both for components and wires
- All components must be easy to access and be able to be removed individually, without dismantling the head (for quick repairs)
- Impact resistant and strong (in comparison to previous design)

6.3.3.2 Easy Access

With 3D printing expertise in the group, it was decided that this would be an appropriate technology to use as it allows the creation of complex geometry to fit each component (Figure 50). ABS plastic was used due to its impact resistance and because it's a standard material for the 3D printing process used (FDM).

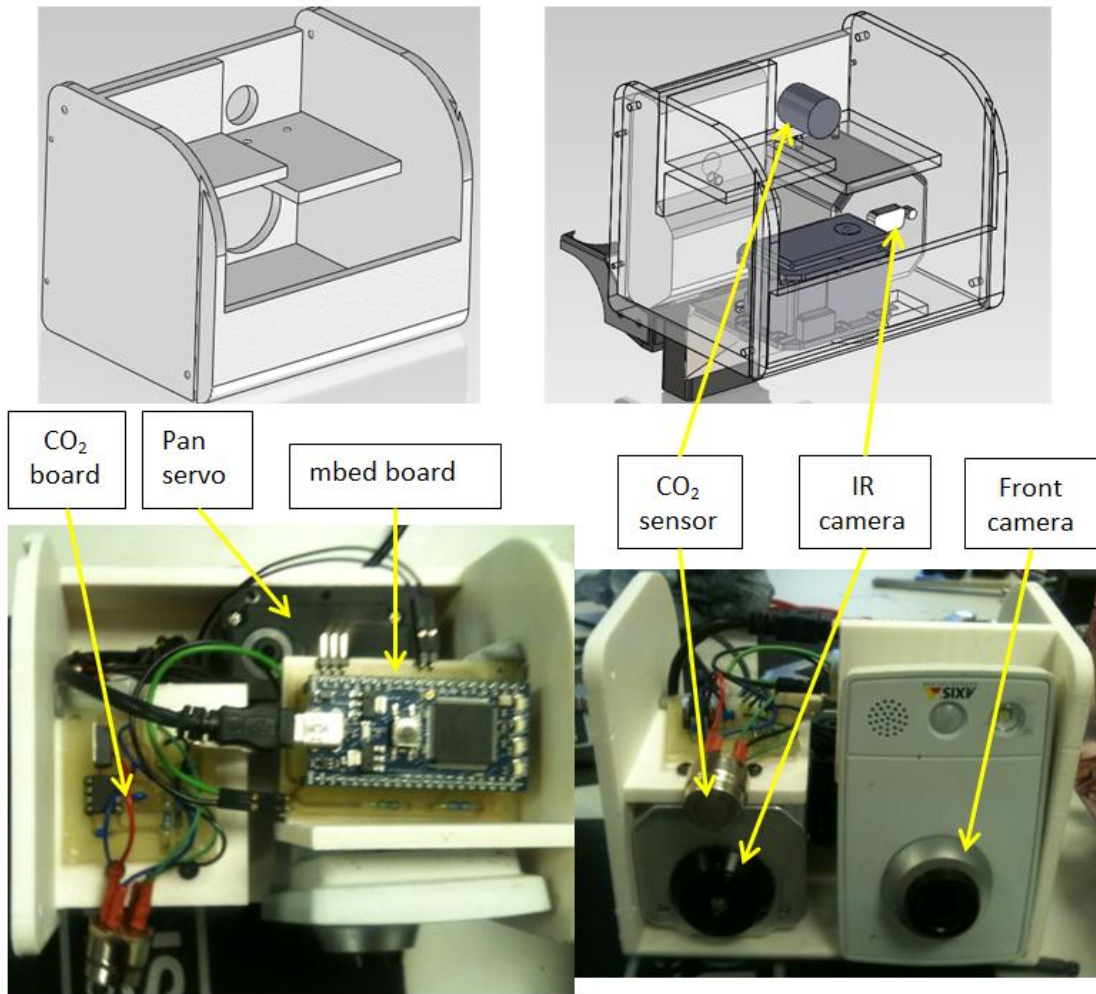


Figure 50. CAD design and finished head assembly.

A removable lid was designed to aid with access to components for maintenance. Using a sliding design rather than a hinge makes the head less susceptible to dust and rainwater (Figure 51).



Figure 51. Sliding lid for easy access to internal components.

6.3.3.3 Weight Reduction

A breakdown of the weight of the original head (excluding cables) is shown in Table 7.

Table 7. Component contributions to initial head weight.

Component	Weight (g)
LiDAR	160
IP Camera	160
Xsens IMU	50
Flir Photon 160	115
USB Hub + Components	50
Rx64 Servomotor	125
Lid + Hinges	80
Aluminium Shell	160
TOTAL	900

A breakdown of the weight (excluding cables) of the new head design is shown in Table 8.

Table 8. Component contributions to redesigned head weight.

Component	Weight (g)
IP Camera	160
<u>Flir</u> Photon 160	115
Rx64 Servomotor	125
Mbed	15
3D Printed Shell	220
TOTAL	635

There is a total mass saving of 29% in the new design which reduces vibrations and makes the head easier for the arm to lift.

6.3.3.4 Size

The head is taller than the previous design (if the LiDAR is excluded) however this is because the IP camera did not fit into the old design. The new design is more importantly thinner and shallower (Figure 52) allowing the head can to achieve 180 degrees of movement in both the tilt and pan without colliding with the arm.

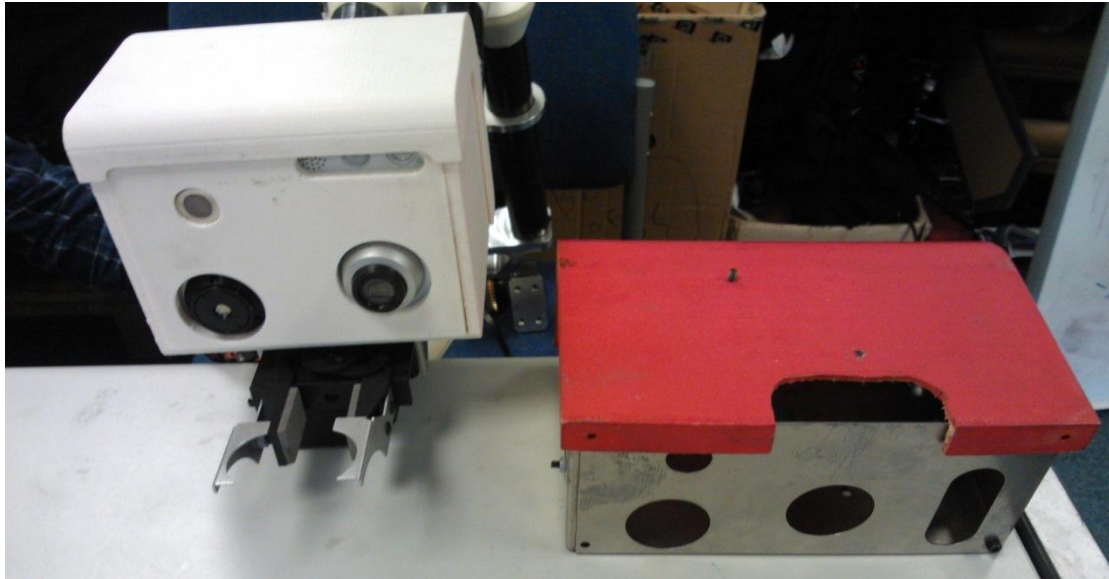


Figure 52. Side to side comparison of 2013 (left) and 2012 (right) WMR robot heads.

6.4 Results

- Head weight reduced by 29% thus minimizing vibrations
- All sensors now operational:
 - LiDAR and CO₂ sensor data displayed in GUI
 - IMU and flipper encoders used for 3D representation
- Gripper is functional and can be controlled by the operator

7 Control system

7.1 Initial State

From the preliminary testing of the robot, as well as advice from the previous year's team, a SWOT analysis of the current control system was performed (Table 9).

7.1.1 SWOT Analysis of Control System

Table 9. SWOT analysis of the initial control system

<p>Strengths:</p> <ul style="list-style-type: none"> • GUI has frames set up for cameras and speed sliders in convenient locations • PS3 controller is ergonomic • The system allows constant communication between the client and server • The system is functional and previously used to good effect in competitions. 	<p>Weaknesses:</p> <ul style="list-style-type: none"> • Code is unreliable – unexpected and unknown errors occur. • Little feedback to the driver (errors and driver aids) • Some functionality missing (CO₂ sensor, 3D representation) • GUI layout is confusing and cluttered – doesn't fit onto different screens • Driver awareness is low – flippers cannot be seen, unknown robot orientation. Previous competition failures caused by lack of awareness. • Controller layout is not intuitive – 6 axis control is complicated and inaccurate • Only joint control is available to move the arm which relies heavily on driver spatial awareness to be effective
<p>Opportunities:</p> <ul style="list-style-type: none"> • Update the 3D representation • Show battery life on the GUI • Improve operator awareness through GUI • Some old working features are still in the code but not implemented and can be updated with minimal work. 	<p>Threats:</p> <ul style="list-style-type: none"> • Lack of coding expertise in the team – some features may need to be simplified • Build-up of many teams work has created a confusing set of sub-systems which are interdependent. • If the code is unchanged, the robot risks uncontrollable errors and drop-outs which will hinder performance

Reliability was highlighted as problem for the previous team, with motors dropping out and communication problems during preliminary testing. Also, the system was not providing the driver with information about surroundings which on previous occasions had caused catastrophic failures (the robot toppling in the 2011 RoboCup competition). It was evident the robot lacked functionality which could be improved through 3D representation and heartbeat to immobilize robot if communication lost.

7.2 Specification

- Provide operator with awareness of the robot's surroundings
- Improve the reliability of the system by preventing motor drop-outs and communications failures
- Improve the intuitiveness of control by remapping the controller layout and improving the arm control
- Make the system easy to learn by automating and simplifying user controls
- Give more information to the driver regarding errors and robot operations

7.3 Architecture

The overall architecture of the software is inherited from previous years (Figure 53).

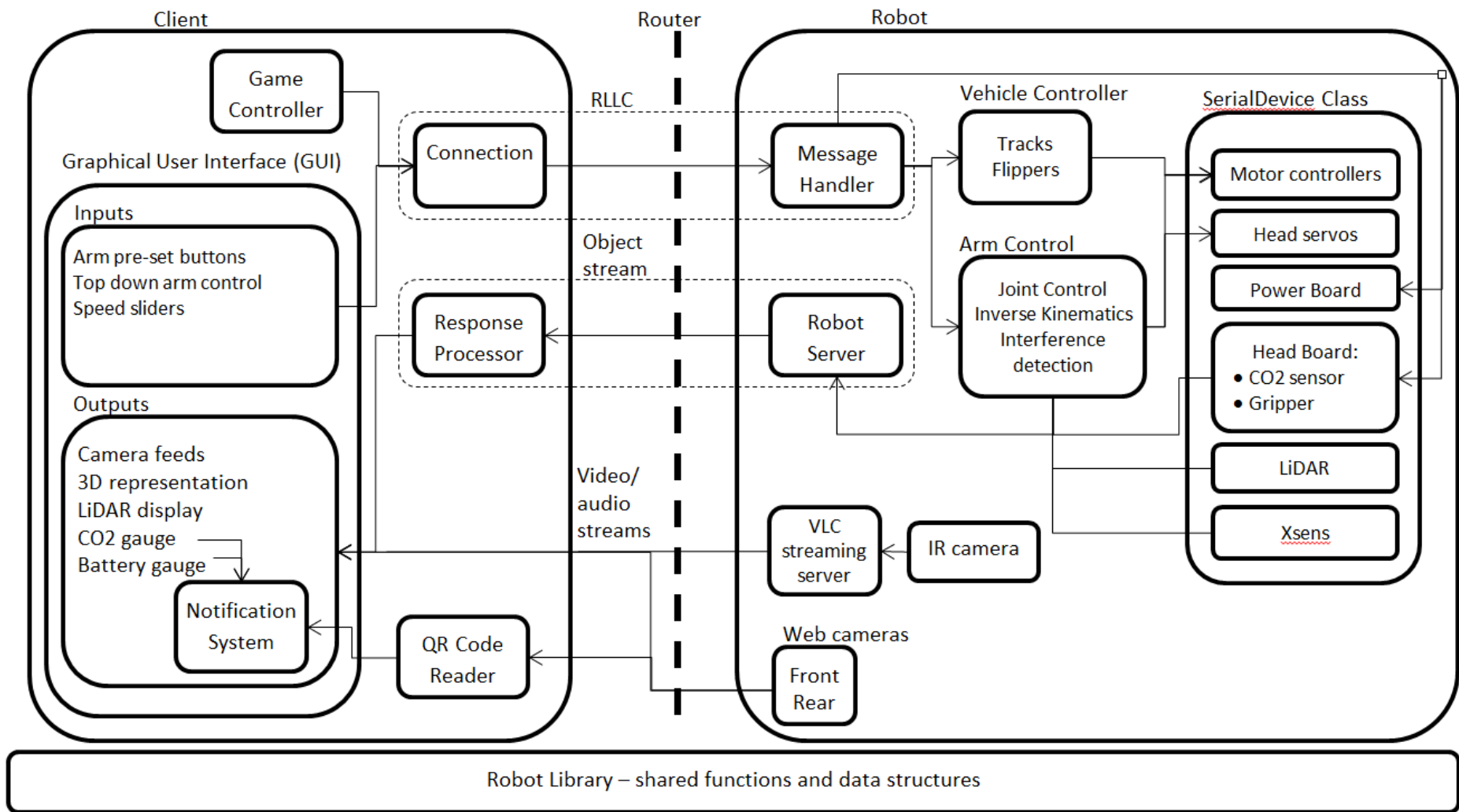


Figure 53. Architecture of the robot control software.

7.4 Graphical User Interface

The GUI is the only method to provide the operator with information about the robot. The SWOT analysis highlighted some weaknesses of the operator interface, the most prominent being the missing features and lack of organisation (Figure 54).



Figure 54. Initial state of the GUI.

The new GUI holds all of the features and resizes with any display (Figure 55). The layout has been improved so that panels are fixed in place and cannot 'float' around the screen.

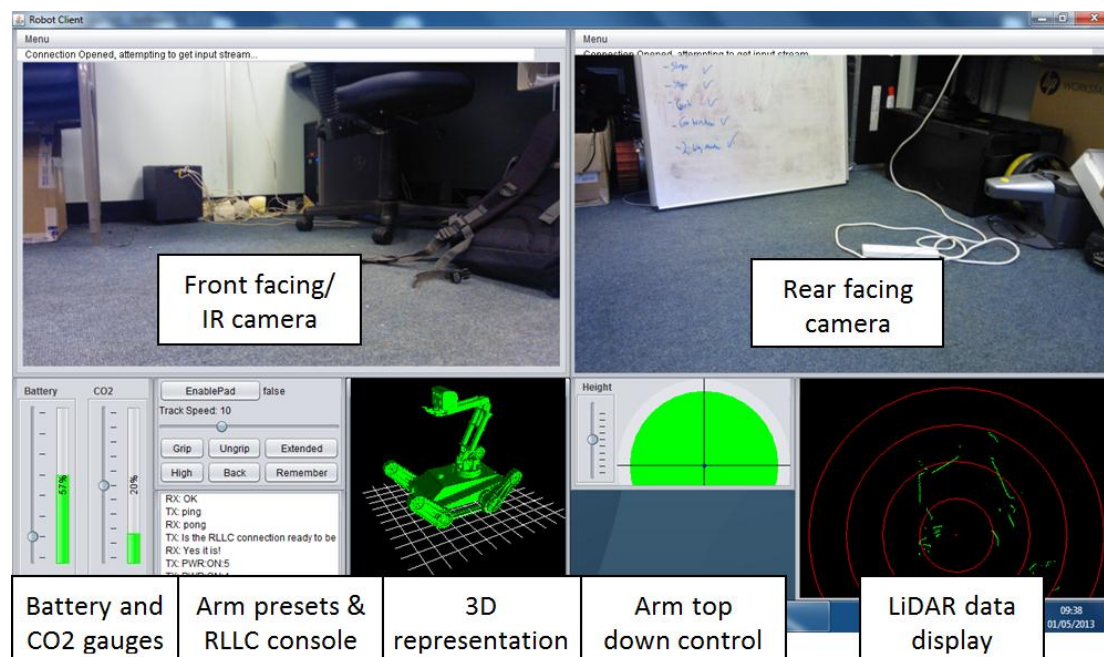


Figure 55. Redesigned GUI layout incorporating new types of feedback.

7.5 Collision System and Error Checking

It was discovered during testing that despite the joints having limits set so that the arm should not crash into itself, there was no function to prevent the arm from colliding with other parts of the robot (Figure 56).

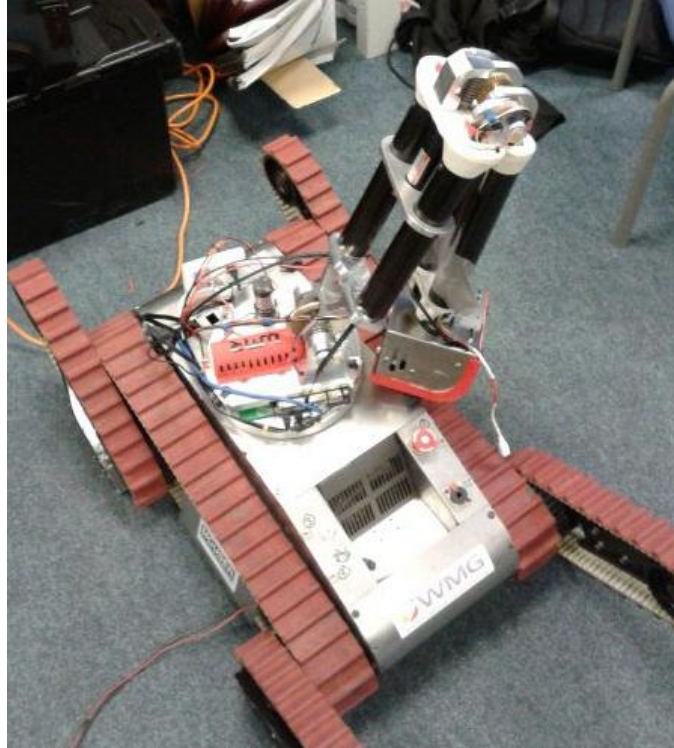


Figure 56. Robot arm crashing into the body using 2012 attempt at inverse kinematics lacking collision detection.

Preventing simple driver errors like surpassing joint limits and colliding with other parts of the robot is crucial to the reliability and ease of use of the system.

7.5.1 Collision Detection

One method of detecting collisions is to calculate positions of each free-body in 3D space and detect whether any intersect. This method is thorough but complex, time demanding and processor intensive. As collision detection was not a critical objective, a quick method to detect collisions was found in Java3D library (Oracle 2013).

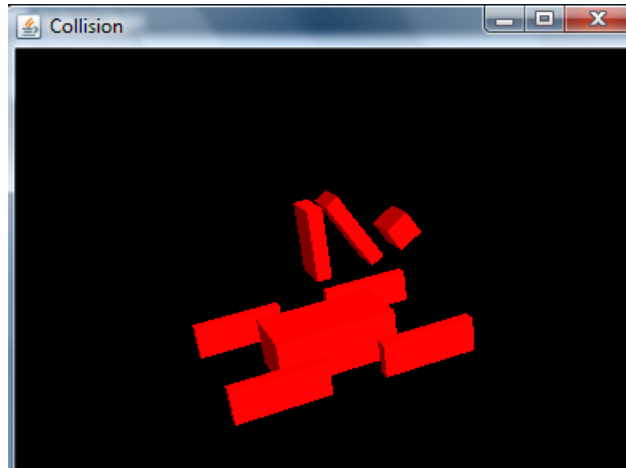


Figure 57. Visualization of the collision boxes used in the collision detection system.

Using this system, a scale model of the robot (with safety factors added) was constructed to run on the server (Figure 57). This detects if a body part is about to collide with another before the command is sent to the motor. If so, the function returns a Boolean error variable and prevents the robot from moving to this position and notifies the operator (Figure 58).

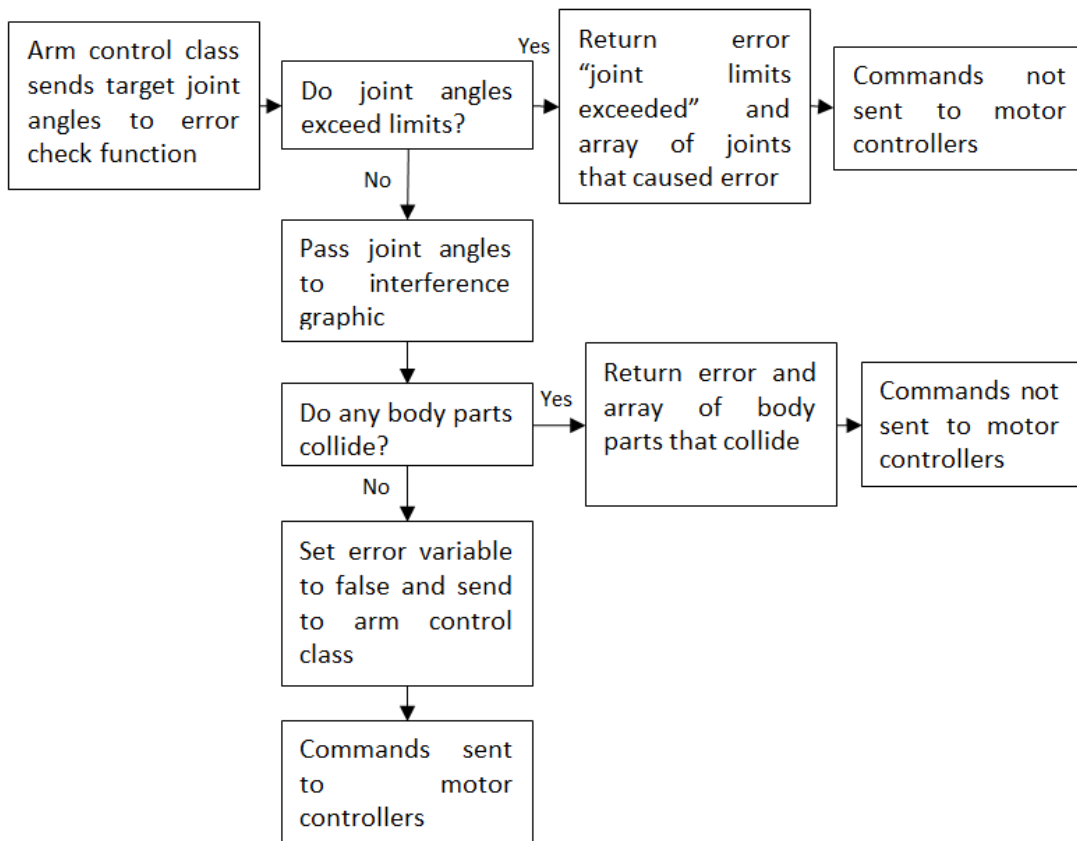


Figure 58. Collision detection algorithm.

7.6 3D Representation

The 3D representation provides the driver with awareness of the robot configuration in space.



Figure 59. 3D representation designed by the 2010 WMR team (not in use last year) (Warwick Mobile Robotics 2010).

An existing 3D representation (Figure 59) was not functional. A SWOT analysis was performed on the previous design, considering the code itself and its suitability to be updated.

7.6.1 SWOT Analysis of 3D Representation

Table 10. SWOT analysis of the existing 3D representation

<p>Strengths:</p> <ul style="list-style-type: none"> • Functionality to show movement of robot arm • Good base design that can easily be adapted 	<p>Weaknesses:</p> <ul style="list-style-type: none"> • Not functional • Does not show flipper positions • The graphic is based on an old design. There is no turret and the lengths are incorrect. • The graphic has unnecessary features. • Code is not streamlined
<p>Opportunities:</p> <ul style="list-style-type: none"> • Show flipper positions • Give feedback on interference, joint limits, robot orientation, centre of gravity • Simplify design to show only important features 	<p>Threats:</p> <ul style="list-style-type: none"> • No speciality in the team for Java3D graphics

The 3D representation was seen as an essential tool for giving the user awareness of the robot and errors that occur when operating remotely. The SWOT analysis highlighted many potential areas of improvement including:

- Adding flippers to the representation
- Visually showing errors
- Providing the user with the orientation of the robot – where the ground is and the angle of the robot.

The threats were considered and alleviated; with one team member being responsible for learning Java3D.

7.6.2 Updates to 3D Representation

7.6.2.1 Graphics

There were many redundant features on the old graphic, such as a sky and arena. These elements have been removed and the design has been streamlined for simplicity of understanding and better contrast in outdoor environments (Figure 60).

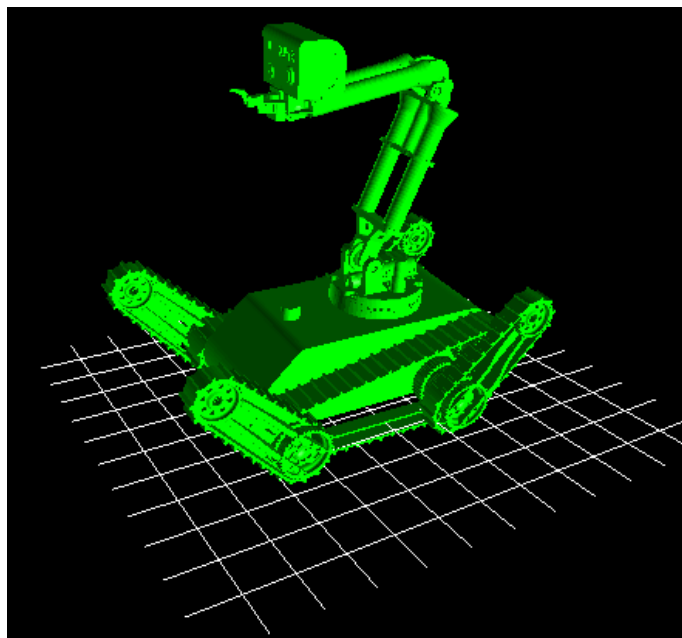


Figure 60. Updated 3D representation graphics

7.6.2.2 Flipper Positions

Previously there was no method other than camera positioning to give the user the flipper positions. Flipper encoder data is now used and the flippers have been added to the 3D

representation, much in the same way as the arm, where positions are stored on the server and then sent across to the client and displayed on the graphic. Having the flipper encoder data also allows the flippers to be included in the collision detection class.

7.6.2.3 Robot Orientation

The orientation data from the IMU has been added to the 3D representation. A grid was used to represent a level ground surface about which the robot rotates (Figure 61). This should help give advance warning of toppling.

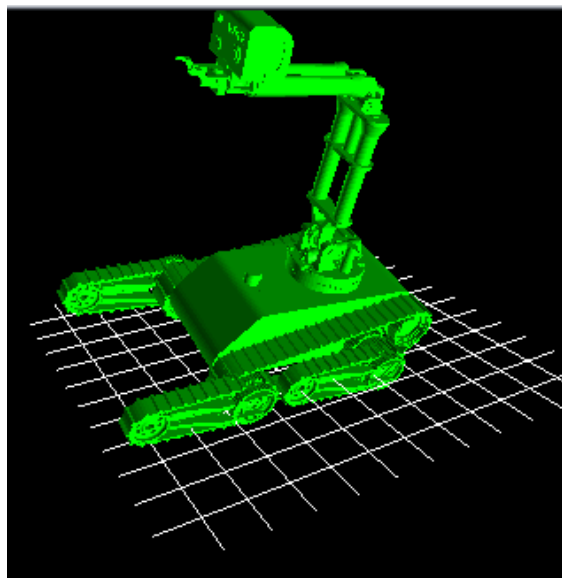


Figure 61. 3D representation showing robot angle with reference to the horizontal plane.

7.6.2.4 Collision

The 3D representation was decided to be the best way to show the user the details of any collisions or joint limits. This was achieved by building in a function which turns the body parts which will collide from green to red (Figure 62).

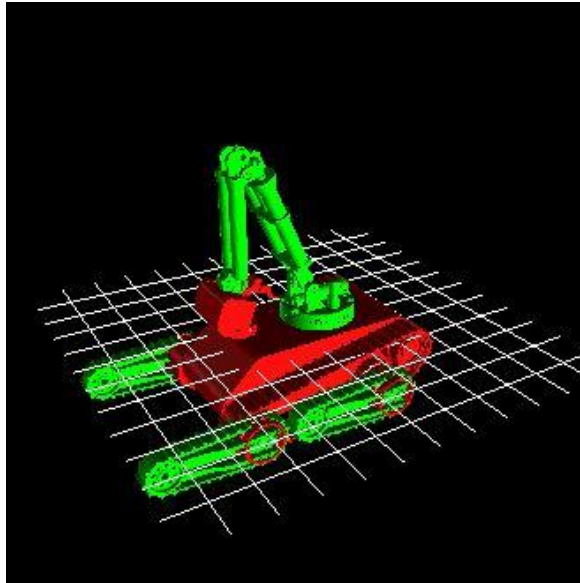


Figure 62. Potential collision highlighted just before occurring.

7.7 Arm Control

Joint-control was the only method to control the arm on the previous design. Initial testing studied the ability of the arm to reach certain positions and the ease at which an inexperienced user could operate the controls.

7.7.1 SWOT Analysis of Arm Control

From initial testing, a SWOT analysis was performed (Table 11).

Table 11. SWOT analysis of existing arm control options

<p>Strengths:</p> <ul style="list-style-type: none"> • Can manipulate the arm into any position • PS3 controller is intuitive • Pre-sets good for quick positioning 	<p>Weaknesses:</p> <ul style="list-style-type: none"> • Arm control requires great spatial awareness • Difficult to remember controls (layout not intuitive) • Cannot dictate the path by which the arm moves, making it difficult to pick up objects • Slow
<p>Opportunities:</p> <ul style="list-style-type: none"> • Increase the number of pre-sets for more scenarios • Implement inverse kinematics 	<p>Threats:</p> <ul style="list-style-type: none"> • The motor controllers use PID control therefore position and speed cannot be set simultaneously. Overshoot Problems.

It was decided to implement inverse kinematics enabling the user to control the position of the end-effector within three-dimensional co-ordinate space, rather than joint control. With this method of controlling the arm the user only has to aim towards the target and the inverse kinematics calculates the joint angles necessary to get there.

The controller layout was also highlighted as an area of improvement to improve the ease of use and speed of learning for new users.

7.7.2 Specification for the New Arm Control System

- Intuitive controller layout: existing functionality as well as new features
- Implement inverse kinematics to allow the user to ‘fly the head’
- Keep track of arm position at all times to allow transition between control methods and provide feedback of arm position to 3D representation
- Smooth motion keeping overshoot to a minimum

7.7.3 Inverse Kinematics

Previous attempts (Warwick Mobile Robotics 2012) used matrix methods to solve the IK equations however this year the two planes of motion have been taken separately and then combined with the equations, making the problem simpler.

7.7.3.1 Cylindrical Co-ordinate Frame

The kinematics was first solved in a cylindrical co-ordinate frame and the transformed into a Cartesian co-ordinate frame. A cylindrical co-ordinate frame was chosen because the arm effectively acts in a two-dimensional plane r - z which is rotated about the z axis by the turret (global angle θ).

Consider the arm moving in just the r - z plane with end-effector co-ordinates p_r and p_z (Figure 63).

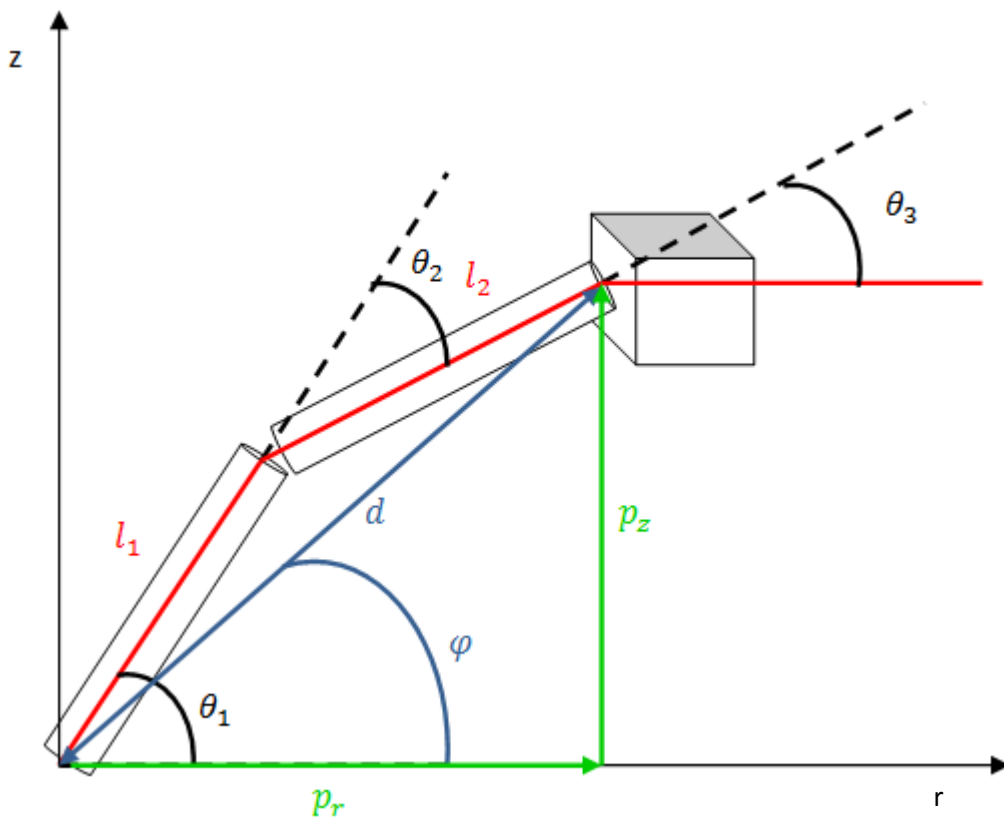


Figure 63. Arm in the Cartesian coordinate frame.

Using Pythagoras, the distance d from the origin and angle φ are calculated in terms of the target positions p_r and p_z :

$$d = \sqrt{p_r^2 + p_z^2}$$

$$\varphi = \tan^{-1}\left(\frac{p_z}{p_r}\right)$$

Using trigonometry, θ_2 , θ_1 , and θ_3 , are calculated:

$$\theta_2 = \cos^{-1}\left(\frac{d^2 - (l_1^2 + l_2^2)}{2l_1l_2}\right)$$

$$\theta_1 = \tan^{-1}\left(\frac{l_2 \sin \theta_2}{l_2 \cos \theta_2 + l_1}\right) + \varphi$$

$$\theta_3 = \text{tilt} + \theta_1 - \theta_2$$

These functions were implemented into the software to calculate the angle of the shoulder and elbow joints (as well as the tilt angle) needed to reach any position in the x-z plane. In a cylindrical co-ordinate system of r-z- θ , the position of the robot arm in three dimensions can now be achieved by setting the turret rotation θ_5 to the global angle θ (Figure 64).

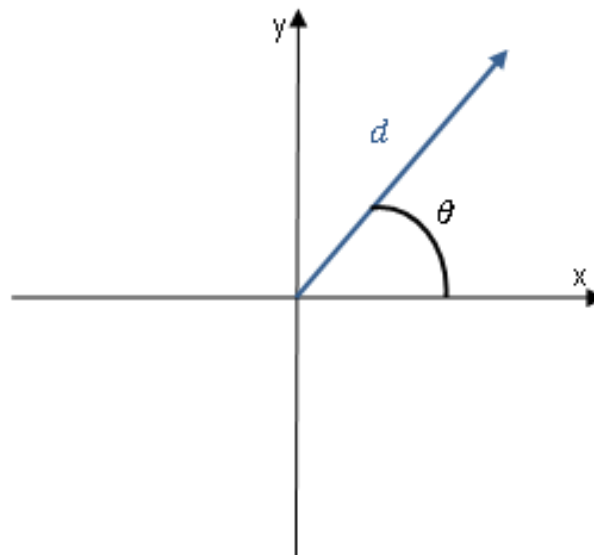


Figure 64. Top down view of the cylindrical coordinate frame.

7.7.3.2 Cartesian Co-ordinate Frame

In order to fly the head in all directions, it was necessary to transform the cylindrical co-ordinate system into a Cartesian system. As both systems have the same z co-ordinate, the only transformation that needs to occur is the two-dimensional transformation from r- θ to x-y.

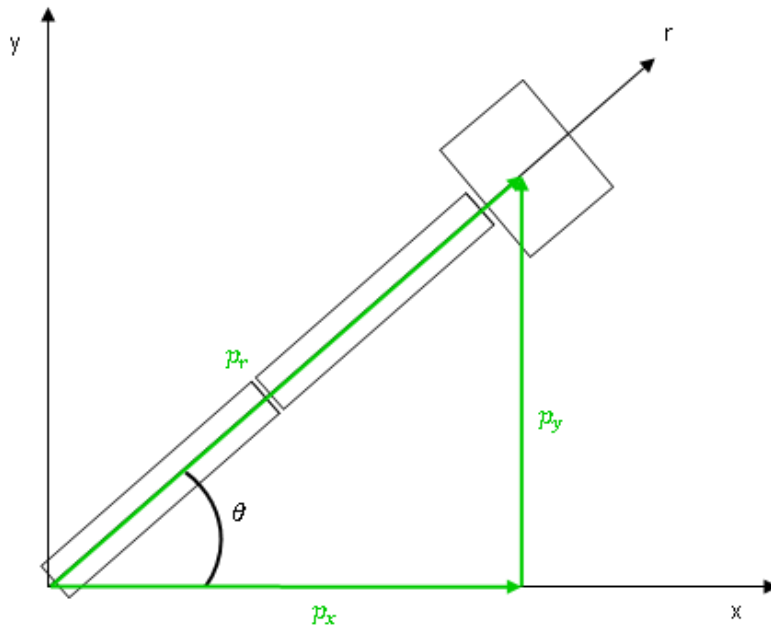


Figure 65 Robot arm top-down view (Cartesian Co-ordinate frame)

From trigonometry:

$$p_x = p_r \cos \theta \text{ and } p_y = p_r \sin \theta$$

These transformations provide all the information needed to find the joint angles to move the head to any x-y-z co-ordinate. If x, y and z co-ordinates are provided, the value of r can be calculated from x and y. The kinematics are then solved in the cylindrical co-ordinate frame and the arm moves.

7.7.3.3 'Flying' the Head

The operator should be able to move directly at a target object that the robot head is facing. This was achieved by creating a new local co-ordinate frame based upon the tilt and pan of the end-effector (see Appendix D.1).

7.7.4 Linear Interpolation

In order to make the movement of the arm smooth and on a straight path, linear interpolation between the current and target point is used for all movements. This simply uses Pythagoras's theorem to calculate a series of points between the target and position

which have small intervals between them, therefore making the arm move in a relatively straight path.

7.7.5 Pre-sets

The previous design had two 'pre-set' positions for the arm which could be accessed from the controller. These allowed the arm to be placed either low-down and protect it during driving whilst the other raised the arm in order to search for targets. These pre-set positions were useful and were adapted to work with the new inverse kinematics code (by setting the pre-sets based on co-ordinate positions rather than joint angles).

An extra pre-set position 'Limbo position' (Figure 66) was devised and added to the GUI—this is both forwards and backwards and allows the arm to be stretched as far as possible straight out in front of the robot.



Figure 66. Robot in "limbo" position under a low table.

As well as adding pre-sets, a new feature this year was created that allows the user to store previous positions of the arm, useful for completing repetitive actions.

7.8 Controller Layout

From initial testing and the SWOT analysis, the controller layout was highlighted as a key improvement area, the unintuitive layout being a major concern.

Four different controller modes were developed (see Appendix D.2 for details):

- Drive mode – for navigating complex terrain
- Inverse kinematics mode – to fully control the arm for gripping/manipulation
- Search mode – mimics controller layout in first-person shooter games
- Joint mode – for backup control of the arm

8 Testing

8.1 Aims

- Compare the modified robot design's performance to the initial design.
- Determine whether the 2013 aims and objectives have been achieved, and to what extent

8.2 Method

A structured testing plan was devised that ensured results obtained were measurable and comparable. The tests assessed both the performance of any new features the WMR team had developed this year (as outlined in this report) and also the performance of the robot in relation to the capabilities required in the RoboCup competition (IEEE Robotics and Automation Society 2013).

The tests were performed at the testing facilities of WMR sponsor, Remotec (Northrop Grumman 2013). This allowed for a more environmentally realistic assessment, with more obstacles than WMR would have had access to at the University.

Two types of tests were conducted:

- Line-of-sight tests where capabilities of the robot only were assessed (Figure 67 (a))
- Remote (blind) tests where operator control interface was assessed (Figure 67 (b))

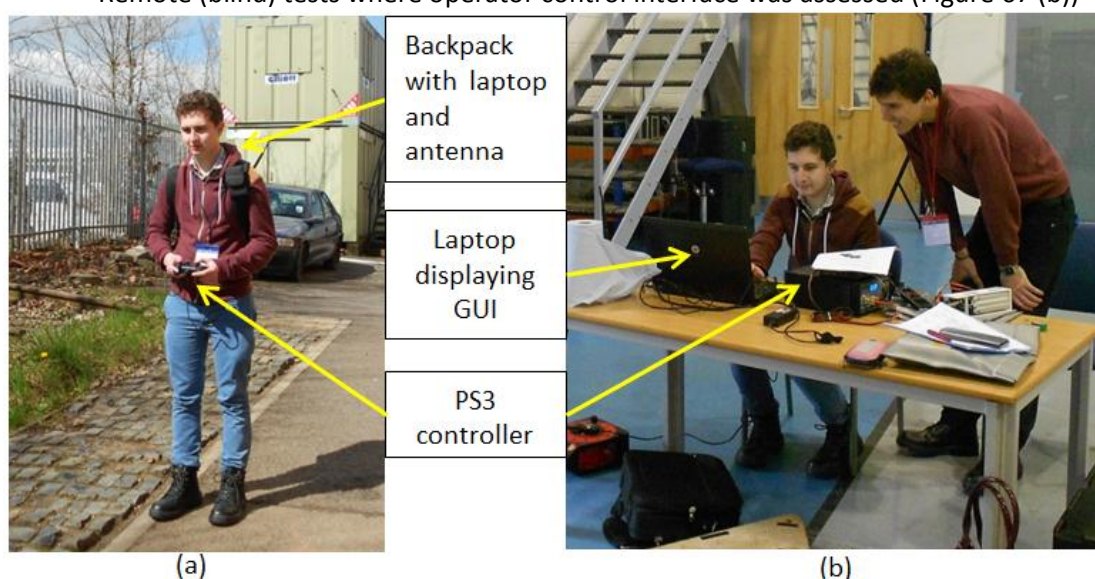






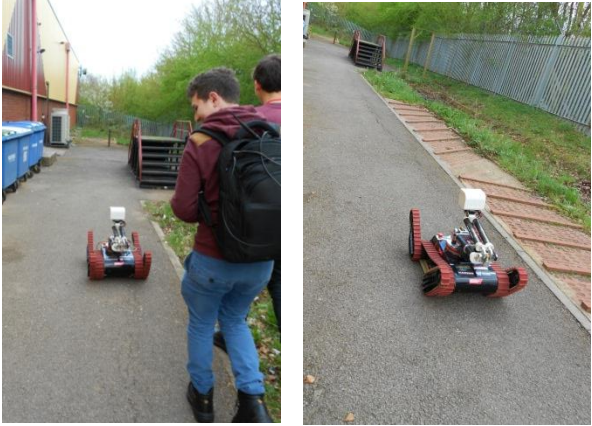
Figure 67. Operator setup (a) for line of sight testing, (b) for remote testing.

8.3 Results

Table 12. Testing results and observations

Challenge	Test relation to Competition	Competition Capability	Definition of Success	Capable?	
<p>Train tracks</p>  <p>(a)</p>  <p>(b)</p> <p>Figure 68. The robot ascending (a) and descending (b) a rail track</p>	<p>Real rubble similar to competition simulated rubble.</p>	<p>Mobility</p>	<p>The robot is able to traverse the train tracks</p>	<p>Yes</p>	
		<p>Notes: Test successful over train tracks testing area. However, once completed and out of test section, the robot locked into forward drive mode and had to be E-stopped.</p>			
		<p>Operator Control</p>	<p>The robot is able to traverse the train tracks when controlled from a remote location</p>	<p>Yes</p>	
<p>Notes: Test successful over train tracks testing area. However, when the robot reached following terrain, mud and twigs were caught between the flippers and tracks; causing a jam. Test was regarded a pass due to:</p> <ul style="list-style-type: none"> • Test assessed mobility and robot was able to traverse rail tracks • Indoor competition, so no mud/twigs would clog the flippers. 					

<p>Uneven pavement</p>  <p>Figure 69. The robot traversing the uneven pavement</p>	<p>Terrain is uneven under competition conditions</p>	<p>Mobility</p>	<p>The robot is able to traverse the uneven road without toppling or inner components becoming dislodged</p>	<p>No</p>
<p>Notes: Test failed due to the power cutting out whilst the robot was travelling over the pavement. A diagnostic afterwards proved this fault to be due to a metal component causing a short circuit on the power board due to vibration.</p>				
<p>Tiled pavement</p>  <p>Figure 70. The robot traversing the tiled pavement</p>	<p>See above: Alternative topography to the uneven pavement</p>	<p>Mobility</p>	<p>The robot is able to traverse the uneven road safely</p>	<p>Yes</p>
<p>Notes: The test failed initially due to significant connection lag. However, the definition for passing this test was focused on the mobility of the robot. The test was passed the second time.</p>				

<p>Range Test Distance: 20m</p>  <p>(a) (b)</p> <p>Figure 71. Operator controlling the robot (a) in line of sight (b) blindly.</p>	<p>Remote driving during competition for long periods</p>	<p>Mobility</p>	<p>The robot is able travel the entire distance without cutting out due to any motor, wiring or battery faults</p>	<p>Yes</p>
<p>Notes: Test passed with no problems encountered.</p>				
		<p>Operator Control</p>	<p>The robot is able travel the entire distance when controlled from a remote location</p>	<p>Yes</p>
<p>Notes: As long as antenna had line of sight no problems were encountered.</p>				

Stairs (38° incline)



(a)



(b)

Figure 72. : (a) Mobility test descent (b) blind ascent with raised arm

Slopes of up to 45° found in competition

Mobility	Robot is able to ascend and descend the stairs without toppling	Yes
Notes: Both the ascent and descent were passed without issues.		
Operator Control	Robot is able to ascend and descend the stairs when controlled remotely	No
Notes: The descent was passed. The ascent test was failed due to a pre-test fault; locking the arm's shoulder joint into an upright position This raised the centre of gravity and caused the robot to topple backwards.		

Ramp (30° incline)



(a)



(b)

Figure 73. (a) Mobility test descent (b) blind descent

Slopes of up to 45° found in competition

Mobility

Robot is able to ascend and descend the ramp without toppling

Yes

Notes: Both the ascent and descent were passed without problems. There was sufficient traction to hold the robot in place.

Operator Control

Robot is able to ascend and descend the ramp with traction, when controlled remotely

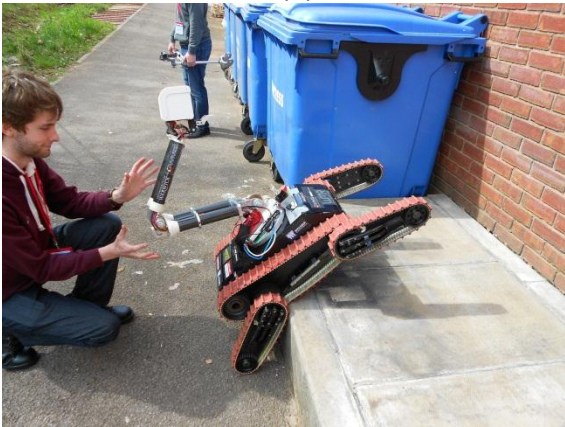
Yes

Notes: Both the ascent and descent were passed without problems – even with the shoulder joint fault.

Curb (300mm)



(a)



(b)

Figure 74. (a) Mobility curb ascent (b) blind curb ascent

Similar to the competition step fields

Mobility

The robot is able to ascend and descend the curb

Yes

Notes: Both the ascent and descent were passed without problems.

Operator Control:

The robot is able to ascend and descend the curb when controlled remotely

No

Notes: The robot toppled on both ascent and descent. This was due to the shoulder joint locking fault. The centre of gravity information provided to the operator did not prevent this failure.

Vehicle observation



(a)



(b)

Figure 75. (a) Manipulation test stage 1 (b) stage 2

In the competition narrow holes must be accessed.

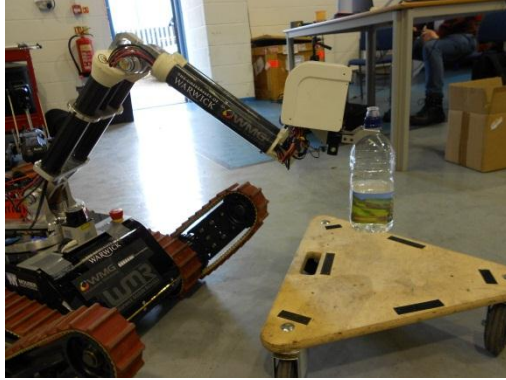
Manipulation

The robot is able to manoeuvre its flippers, arms and head to observe into a vehicle through an open window.

Yes

Notes: Due to lack of operator experience, this test was performed slowly but the objective of accessing the inside of a vehicle was achieved

Water bottle gripping (750mm table)



(a)



(b)

Figure 76. (a) Placing water bottle in a target area (b) gripping bottle from table

Gripper capabilities will be tested in the competition

Manipulation	The gripper is able to grip the bottle from a height before releasing it on a target.	Yes
Notes: Some initial difficulty manipulating the head to the correct position, the gripper itself had smooth transitions between the set increments of opening/closing.		
Operator Control	The gripper is able to grip the water bottle from a before placing on a target, whilst being operated remotely.	No
Notes: This test was performed in the car, from the same height as the manipulation challenge. The task was failed due to the robot not being driven close enough to the car (operator inexperience). Therefore when the arm was fully outstretched to reach the bottle, it could not reach the target without surpassing joint limits.		



Figure 77. Blind gripper test from car seat

Small steps
Maximum step height: 200mm

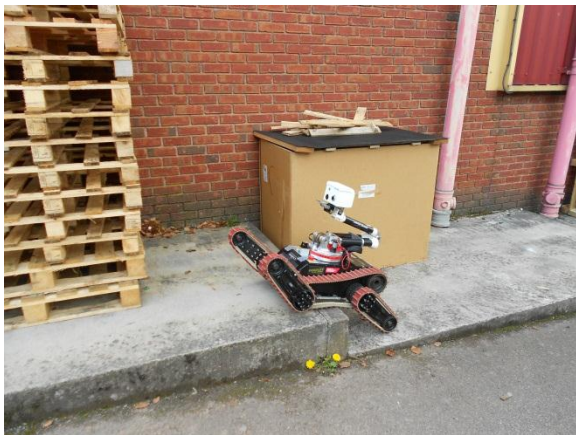


Figure 78. Small step mobility test ascent

Basic terrain
navigation
preparation for
competition

Mobility

The robot was easily and quickly able to ascend these obstacles without toppling

Yes

Notes: Test was passed quickly and no problems encountered.

8.4 Analysis of Results

Most mobility, manoeuvrability and manipulation tests were passed. The exceptions to this were the uneven pavement negotiation, blind curb and stairs ascents and the blind water bottle test.

The uneven pavement test was least strongly correlated to the competition tasks. Therefore, its failure was not critical to the team. Although the robot is required to negotiate complex terrains that simulate disaster zones in the competition, this particular pavement topography is not directly assessed. However, designing for resistance to vibrations is strongly advisable so a “flight check” of all connections and components inside the robot should be carried out before each run. This test was one of the first conducted; so the fact that the robot continued through testing after undergoing such vibrations shows robustness.

The blind curb and stairs ascent tests were failed due to a pre-testing fault that damaged the shoulder motor and caused the arm’s shoulder joint to lock into an upright position. This raised the centre of gravity, made the robot unstable and caused toppling. As one of WMR’s key aims was to improve the reliability, it was deemed these were two serious fails. In order to remedy this issue before the competition, the elbow joint will be repaired and the code modified to include more rigorous joint limits.

The line-of-sight bottle test was successful. As this is a direct requirement of the competition, the points for the challenge would have been awarded.

The blind bottle test was failed: The operator misunderstood how close the tracks were to the car. This led to not being able to reach the bottle. Therefore, additional operator practise is required until this task can be performed reliably.

The testing has provided a good prediction for how the robot will perform at the competition, as many of the tasks carried out will need to be repeated at the RoboCup. As extensive structured testing has not been performed by other WMR teams before, this not

only prepares this year's team for the competition but also allows for a benchmark for next year's team to measure progression.

Whilst at Remotec feedback was obtained from their Programme and Future Development Manager, Peter Green. He was impressed and said that "the WMR system performed well for its first time out; the railway lines were negotiated with little effort followed by some off-roading and then stairs all within minutes of arrival. As the day went on driver confidence grew and negotiation of terrain and use of arm became second nature." (Appendix E.1 full quote).

9 Critical Review

The chassis redesign has significantly reduced the weight of the structural components but the overall weight of the robot is still around 40kg due to the heavy arm and motors. Reducing this would increase battery life. The shifted centre of mass allows for easier climbing of steep inclines, with the arm in the stowed position. With the arm damaged and immobile (as it was during testing) robot mobility is hampered. Chassis strength has proved to be sufficient in most directions. An unforeseen sideways loading due to excessive track tension (caused by ingress of dirt) caused some deformation in the chassis side. This can be remedied by adding cross-bracing at the back of the chassis. Furthermore, techniques to keep the tracks clean of rubble should be investigated.

The improved power system has performed reliably. This is expected to have a very positive impact on competition performance as wiring problems and sensor drop-outs have traditionally been an issue. Designing and manufacturing a reliable wiring harness has been one of the most difficult tasks this year. While the current design performs well it is difficult to modify and certainly difficult to comprehend for someone who has not been involved in the process. It is suggested that in the future specialist technical advice on wiring harness design be sought; one solution would be to use SolidWorks Routing plug-in (Dassault Systemes 2012). The newly developed battery housings enable much easier, safer and faster replacement of batteries. Unfortunately, the new battery monitoring system was not functional during testing due to a communications fault. This will be investigated in more detail before the competition, but as a contingency the old battery monitor can still be utilized.

Overall the reliability of the robot has been improved. The start-up was fairly consistent, with all functions working on the majority of occasions. Therefore, the objective “improve reliability of the system” has been achieved.

The cost-effective approach of using existing sensors to full extent rather than purchasing new ones has paid off. LiDAR raw data has proven to be a useful driving aid to ascertain distances to obstacles. Similarly, integrating the IMU data in the 3D representation aids the operator to avoid toppling. The existing gripper has also proved to be useable, although operator training is crucial to perform gripping tasks reliably. The CO₂ gas sensor has been unreliable, as it tends to produce random voltage spikes and has long settling times. Running the warning system on a moving average value instead of the immediate could be useful.

Control lag was observed during testing when the robot was behind a metal staircase. Generally, the current range of the robot is too small for real-world disaster scenarios. Improved antennae and transmitters should be investigated. One approach would be to move the router from the arm base to the inside of the robot and have a set of external antennae.

A key improvement this year has been the revamped control interface. Providing as much information as possible in a clear and comprehensible way to the operator is crucial to carry out successful remote operations. This was accomplished by a 3D representation and a LiDAR data display. Additionally, “search mode” controller layout combined with working inverse kinematics enables an extremely intuitive control. Nevertheless, operator training is still crucial. For example, an understanding of how to best use the flippers when overcoming obstacles can only be acquired through experience. Flipper presets and simple autonomous behaviours (e.g. “climb step”) could be designed to assist with this. The mobility, manoeuvrability and manipulation capabilities of the robot have remained fairly consistent from last year. Overall the objective “improve operator control” can be assessed to have been a success.

Through performing the testing in a real world scenario, the team was able to assess how well the robot could cope with the elements. Successful features included an enclosed shell and internal battery enclosures, which kept out spots of rain during the test. However, the

robot was not able to cope with the mud and leaves that got caught in the flipper tracks after the rail track test. Debris entering the track system will exert some forces on the chassis that static stress modelling will not show. Therefore, this objective “progress to real world readiness” has only been partly successful.

The testing shows that the robot is performing well overall when compared to last year’s design and also against the competition specifications. It can therefore be concluded that the team has made good use of the sponsorship given this year. The materials bought with money donated by the sponsors have been carefully planned, and this is reflected by the high performance demonstrated through testing.

Throughout manufacture and testing, several potential improvements for the robot were identified (see Appendix E.2 for details).

10 Conclusions

WMR 2013/2013 has been working to address key weaknesses in the tele-operated robot design. The reliability of the system has been improved by redesigning the chassis and head to reduce vibrations and eliminating recurring problems. Additionally, safety of the system has been increased by developing an easy-to-use battery-pack.

Reuse of existing sensors to provide increased operator awareness has been a cost effective way to produce a marked improvement in robot remote operation performance. This was also boosted by a revamped controller layout and GUI, which allows the operator to fully exploit the newly-developed inverse kinematic capabilities.

A full system test in a realistic outdoors scenario has been carried out at Northrop Grumman Remotec facility. This showed good overall performance corresponding to the aims and objectives of the project and the competition specification. The materials purchased with money donated by the sponsors have been carefully planned, and this is reflected by the high performance demonstrated through testing. This serves as a basis for the prediction of good performance in the 2013 World RoboCup Rescue championship.

11 References

- alu Select. *Mechanical Properties EN AW-6082*. 2013.
http://aluminium.matter.org.uk/aluselect/09_mech_browse.asp? (accessed April 28, 2013).
- Anderson Power Products. *SBS Touch Safe 2-3 Pole Connector with Auxiliary*. 2012.
<http://www.andersonpower.com/products/multipole-sbs.html> (accessed December 5, 2012).
- Axis Communications. *Axis M1054 Network Camera*. 2013.
http://www.axis.com/products/cam_m1054/ (accessed April 21, 2013).
- Bay Plastics Ltd. *Plastic Fabrication: Industrial & Commercial*. 2013.
<http://www.bayplastics.co.uk/fabrication.htm> (accessed April 14, 2013).
- Dassault Systemes. *SolidWorks Routing Overview*. 2012.
http://help.solidworks.com/2012/English/SolidWorks/sldpiping/c_routing_overview.htm (accessed April 21, 2013).
- Diginfonews. "Active Scope Camera For Use In Emergency Situations : DigInfo." *Youtube*. 10 June 2008. <http://www.youtube.com/watch?v=djreEBKWPSw> (accessed April 10, 2013).
- EasyCap. *Introducing EasyCap*. 2013. <http://www.easycap.co.uk/> (accessed April 21, 2013).
- Elmira. *Elmira Bio-Based Technology*. 2013. <http://www.elmira.co.uk/> (accessed April 14, 2013).
- FLIR Systems Co Ltd. *Photon 160*. 2012.
http://www.flir.com/uploadedFiles/CVS_APAC/Cores_and_Components/Photon%20160%20R-V-Asia%20LR.pdf (accessed April 21, 2013).

- Franklin, Johnathon. *Trapped Chilean miners found alive - but rescue will take four months*. 23 August 2010. <http://www.guardian.co.uk/world/2010/aug/23/trapped-miners-alive-chile> (accessed April 9, 2013).
- Futurlec. *Technical Information - Carbon Dioxide Sensor*. 2013. http://www.futurlec.com/CO2_Sensor.shtml (accessed April 21, 2013).
- Graber, Thorsten, Stefan Kohlbrecher, Johannes Meyer, Karen Petersen, and Oskar von Stryk. "RoboCupRescue 2011 - Robot League Team Hector Darmstadt (Germany)." *SIM*. 2011. http://www.sim.informatik.tu-darmstadt.de/publ/download/2011_tdp_hector.pdf (accessed April 17, 2013).
- Hector Darmstadt. *Hector GV*. 2012. <http://www.gkmm.tu-darmstadt.de/rescue/?q=node/3> (accessed April 17, 2013).
- Hitec. *HS-422 Deluxe Standard Servo*. 2013. <http://www.hitecrd.com/products/servos/analog/standard-sport/hs-422.html> (accessed April 21, 2013).
- Hokuyo Automatic Co. *Scanning range finder (SOKUIKI sensor)*. 2009. http://www.hokuyo-aut.jp/02sensor/07scanner/urg_04lx.html (accessed April 21, 2013).
- IEEE Robotics and Automation Society. "RoboCupRescue Robot League Rules for 2013." *SSRR Summer School*. 18 January 2013. <http://wiki.ssrrsummerschool.org/doku.php?id=rri-rules-2013> (accessed March 16, 2013).
- Kolbrecher, S., and J. Meyer. *ROS package summary: hector_slam*. 2013. http://www.ros.org/wiki/hector_slam (accessed April 21, 2013).
- KS Composites. *About Us*. 2013. http://www.kscomposites.com/index.php?option=com_content&view=article&id=14&Itemid=60&lang=en (accessed April 14, 2013).

- Lankhorst Pure Composites b.v. *PURE*. 2013. <http://www.pure-composites.com/> (accessed April 14, 2013).
- Maxon motor ag. 2013. <http://www.maxonmotor.com/maxon/view/content/company> (accessed February 14, 2013).
- mbed. *mbed NXP LPC1768 Getting Started*. 2013. <https://mbed.org/handbook/mbed-NXP-LPC1768-Getting-Started> (accessed April 21, 2013).
- . *Prototype your product*. 2013. <http://mbed.org/prototype/> (accessed April 30, 2013).
- Northrop Grumman. 2013. <http://www.northropgrumman.com/uk/> (accessed February 14, 2013).
- . *Remotec Robotic Platforms and Sub-Systems*. 2013. <http://www.northropgrumman.com/Capabilities/Remotec/Pages/default.aspx> (accessed April 29, 2013).
- Nosowitz, Dan. *Earthquake Rescue Robots*. 3 March 2011. <http://www.popsci.com/technology/gallery/2011-03/earthquake-rescue-robots> (accessed April 10, 2013).
- Oracle. *Java SE Desktop Technologies*. 2013. <http://www.oracle.com/technetwork/java/javase/tech/index-jsp-138252.html> (accessed April 2013, 21).
- Pellenz, J. *RoboCupRescue Robot League Rules for 2013*. 2013. wiki.ssrrsummerschool.org/doku.php?id=rrl-rules-2013 (accessed April 3, 2013).
- Phidgets Inc. *What are Phidgets?* 2013. <http://www.phidgets.com/> (accessed April 21, 2013).

- Press Trust of India. *Army acquires indigenous mobile robot 'Daksh'*. 2011. <http://ibnlive.in.com/news/army-acquires-indigenous-mobile-robot-daksh/213477-11.html> (accessed April 29, 2013).
- RoboCup Federation. *Robot League*. 2013. http://wiki.robocup.org/wiki/Robot_League (accessed April 3, 2013).
- RoboCup. *Rescue Robot League Results*. 2012. http://www.robocup2012.org/comp_RCRescue-robot-Results.php (accessed April 17, 2013).
- Roboteq. *AX3500: 2x60A/1x120A*. 2013. <http://www.roboteq.com/brushed-dc-motor-controllers/ax3500-dual-60a-brushed-dc-motor-controller> (accessed April 21, 2013).
- ROBOTIS. *RX-64*. 2010. http://support.robotis.com/en/product/dynamixel/rx_series/rx-64.htm (accessed April 21, 2013).
- S&S. *ABS Material Data Sheet*. 2013. <http://www.sselec.com/data/ins%20specs/ABS%20Data%20sheet.pdf> (accessed April 14, 2013).
- School of Engineering. *Engineering Data Book*. 6th Edition. 2008.
- Shahri, A. M, et al. "RoboCupRescue 2011 - Robot League Team MRL Rescue Robot (Iran)." *Vahid Khorani*. 2011. http://vahidkhorani.com/wp-content/uploads/2012/11/RRL_MRL_TDP.pdf (accessed April 17, 2013).
- SKF. *Deep groove ball bearings, single row*. 2013. <http://www.skf.com/group/products/bearings-units-housings/ball-bearings/deep-groove-ball-bearings/single-row/index.html?prodid=1010281903> (accessed April 28, 2013).
- Tadokoro, Satoshi. *Rescue Robotics : DDT Project on Robots and Systems for Urban Search and Rescue*. London: Springer, 2009.

- Texas Instruments. *1s to 16s Impedance Track Fuel Gauge | Battery Gas Gauge*. 2013. http://www.ti.com/product/bq34z100?DCMP=analog_power_mr&HQS=bq34z100-pr-eu (accessed April 21, 2013).
- . *Standalone 4-10 Cell Precision Protector for Li-Ion Chemistries*. 2012. <http://www.ti.com/product/bq77910a> (accessed April 21, 2013).
- The Imagineering Foundation. *Fairs*. 2012. <http://imagineering.org.uk/fairs/information/> (accessed April 2, 2013).
- VECNA. *Bear*. 2013. <http://www.vecna.com/innovation/bear> (accessed April 10, 2013).
- Vishay. *Model 357 product information*. 2009. <http://www.vishay.com/resistors-variable/list/product-57059/> (accessed April 21, 2013).
- Warwick Mobile Robotics. *Technical Report*. School of Engineering. University of Warwick, 2010.
- Warwick Mobile Robotics. *Urban Search and Rescue Robot*. ES410 Group Project Technical Report, School of Engineering, University of Warwick, 2012.
- World Nuclear Association. *Fukushima Accident 2011*. 2 April 2013. http://www.world-nuclear.org/info/Safety-and-Security/Safety-of-Plants/Fukushima-Accident-2011/#.UW_2yit37l2 (accessed April 9, 2013).
- WRevGP. *Electric Vehicle Grand Prix (evGP)*. 2013. <http://www2.warwick.ac.uk/fac/sci/eng/meng/warwickracing/evgp/> (accessed April 14, 2013).
- Xsens Technologies B.V. *MTi*. 2013. <http://www.xsens.com/en/general/mti> (accessed April 21, 2013).
- Youngblood, J. *Associate Professor of Materials Engineering at the University of Purdue. Visiting Professor at Warwick. Personal communication*. 27 November 2012.

<https://engineering.purdue.edu/MSE/People/ptProfile?id=11541> (accessed April 14, 2013).

Appendices

Appendix A: Chassis supporting data and calculations

A.1 Physical and virtual drop test results

A.1.1 Physical Testing

High-speed footage (Figure 79) was recorded during the physical tests to enable detailed analysis of impact behaviour. The footage shows the large vibrations on the front flippers when they hit the floor. Similarly, flexing in certain point in the chassis was observed, which led to excessive vibrations of the arm and the head.

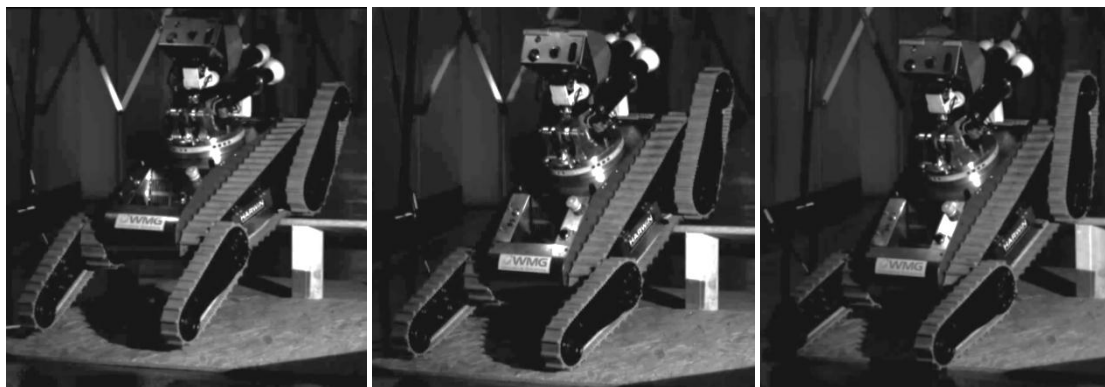


Figure 79. Time-lapse from high-speed footage of a drop test. Full video available on <http://www.youtube.com/watch?v=okQl-gE5u3M&hd=1>

The accelerometer data (Figure 80) shows a maximum peak of acceleration of around 41ms^{-2} , which then reduces in a decaying exponential envelope before becoming steady once more.

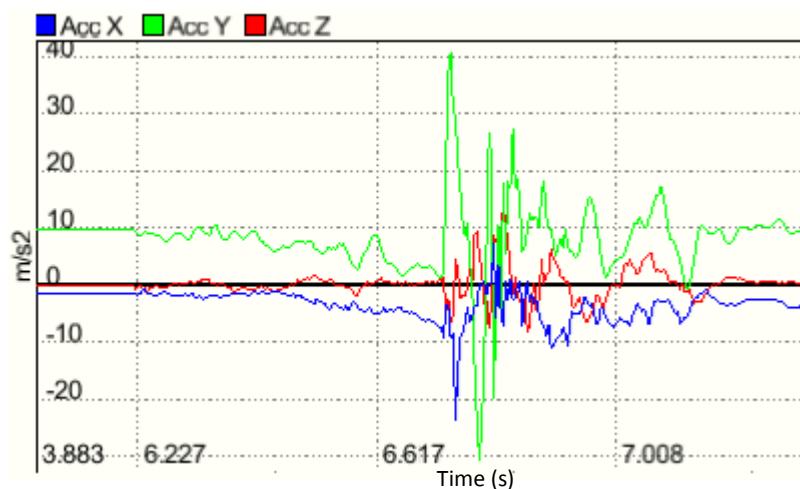


Figure 80. Sample accelerometer data from a drop test.

A.1.2 Virtual Testing

A virtual model was set up in SolidWorks (Figure 81) replicating the physical tests carried out.

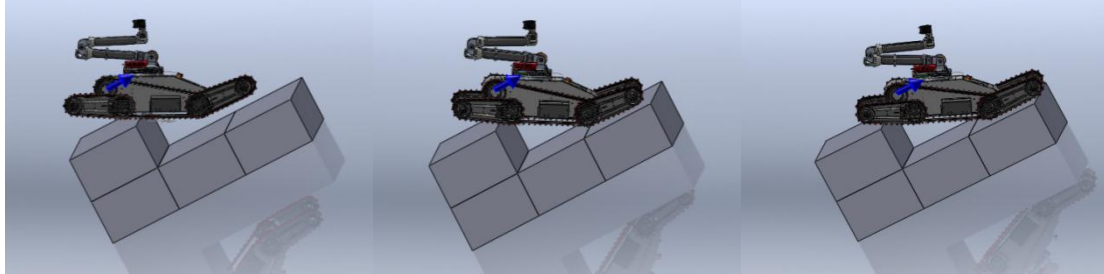


Figure 81. Time-lapse of a SolidWorks drop test.

It was found (Figure 82 (a)) that the maximum acceleration closely matches that found in the physical tests. The maximum force on the right flipper (that which hits the floor first) was found to be 1520N (Figure 82 (b)).

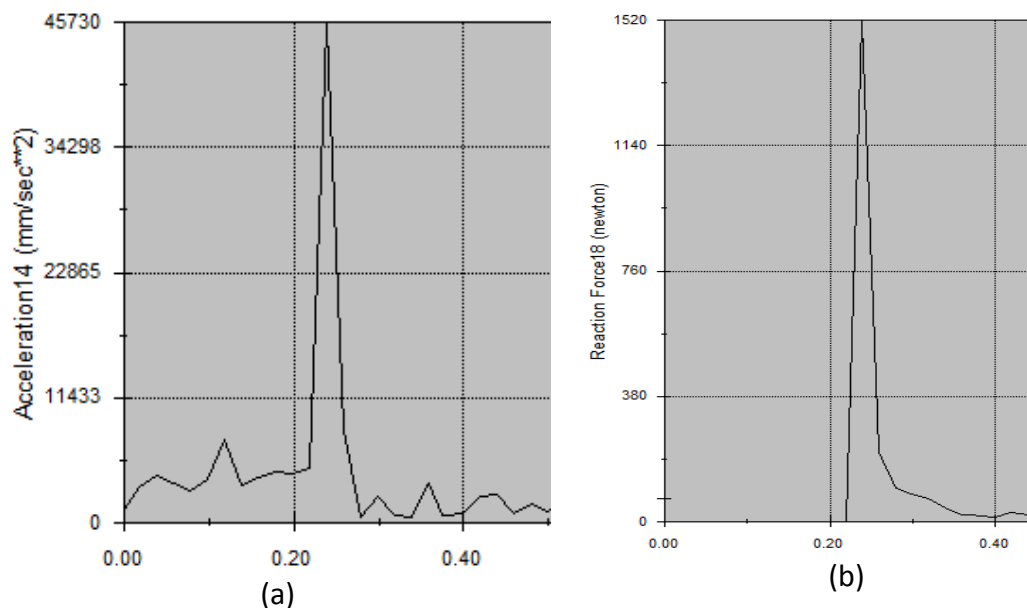


Figure 82. Sample virtual drop test results: (a) Peak acceleration, (b) Peak force

In order to calculate the maximum force encountered by the flipper brackets going through the main body of the chassis, the following calculation was adopted:

$$\begin{aligned}
 &\text{maximum force on flipper} * \text{length of flipper} = \\
 &= \text{sprocket diameter} * \text{maximum force on flipper clamps} \\
 &1520\text{N} * 0.3\text{m} = 0.025\text{m} * F \\
 &F = 18240\text{N} = 18.24\text{kN}
 \end{aligned}$$

It should be noted that the forces calculated by SolidWorks are likely to be higher than in reality because of the need to model the body rigidly that does not account for some force being absorbed by the flippers deforming elastically.

A.2 Space frame FEA results

The final chassis design is shown below in Figure 83. Compared to the chassis for the 2012 team it was found that the difference in mass was 1kg (23% weight reduction).

The strength of the new space frame sides were tested in SolidWorks Simulation. The model had to be simplified as the software was unable to compare the whole assembly including the fixings. Table 13 shows the results of these tests.

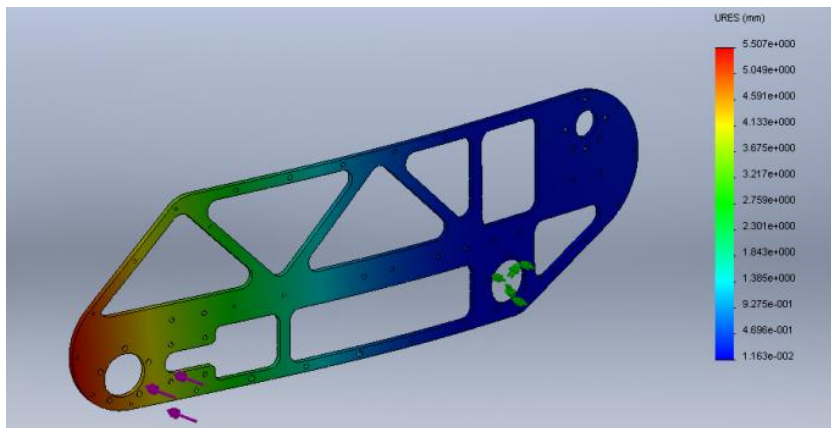


Figure 83. Final space frame deformation under side load.

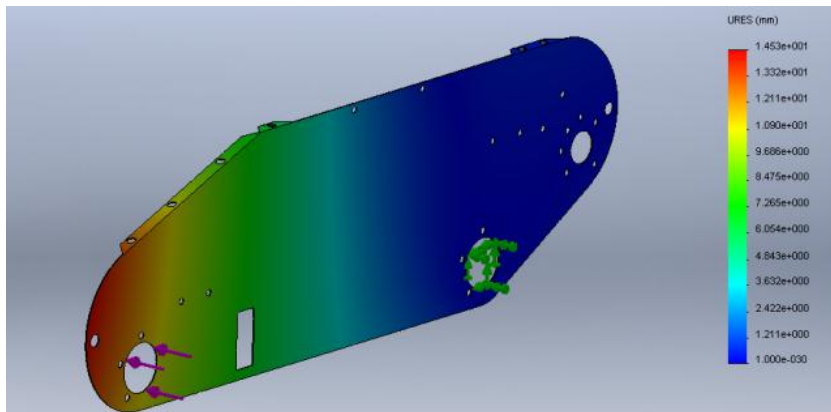


Figure 84. Old chassis side under side load.

Table 13. FEA results comparing the old and the new chassis side

Direction of force	Design	Deflection (mm)	Percentage of yield strength of material
Force applied from front (compressing the frame)	New	0.0012	0.14%
	Old	0.011	0.28%
Force applied from above (compressing the frame)	New	0.0026	0.13%
	Old	0.089	0.78%
Side force on the front and	New	5.51	12.84%

fixed at the back	Old	14.5	189.69%
-------------------	-----	------	---------

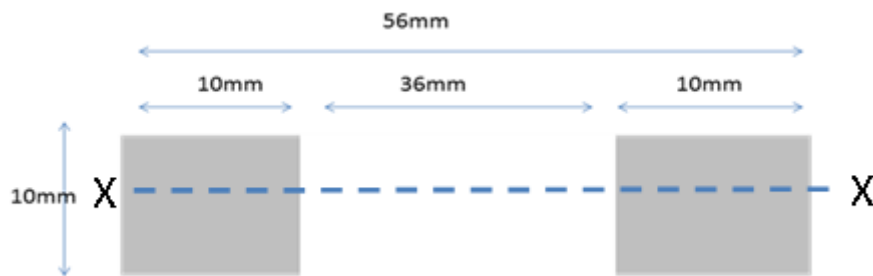
It can be seen from the table that the new chassis stronger in all directions, especially when a sideward force is applied. This is the most important direction as the robot was suffering from the chassis deformation permanently and thus excessive vibrations where caused. By increasing its strength in this direction with a high yield material and strong frame this should be avoided, and protect some of the vital electronics which could suffer.

A.3 Flipper bracket load estimation

Table 14. Variables used in the calculation

Parameter	Definition
W	Force (F)
I	Second moment of area (m ⁴)
y	Distance from neutral axis (m)
L	Length (m)
σ	Yield stress (Pa)
a	Thickness (m)
b	Width (m)
M	Bending moment (Nm)

A.3.1 Rear bracket



$$I = 2 \times \frac{0.01 \times 0.01^3}{12}$$

$$I = 1.66 \times 10^{-9} \text{ m}^4$$

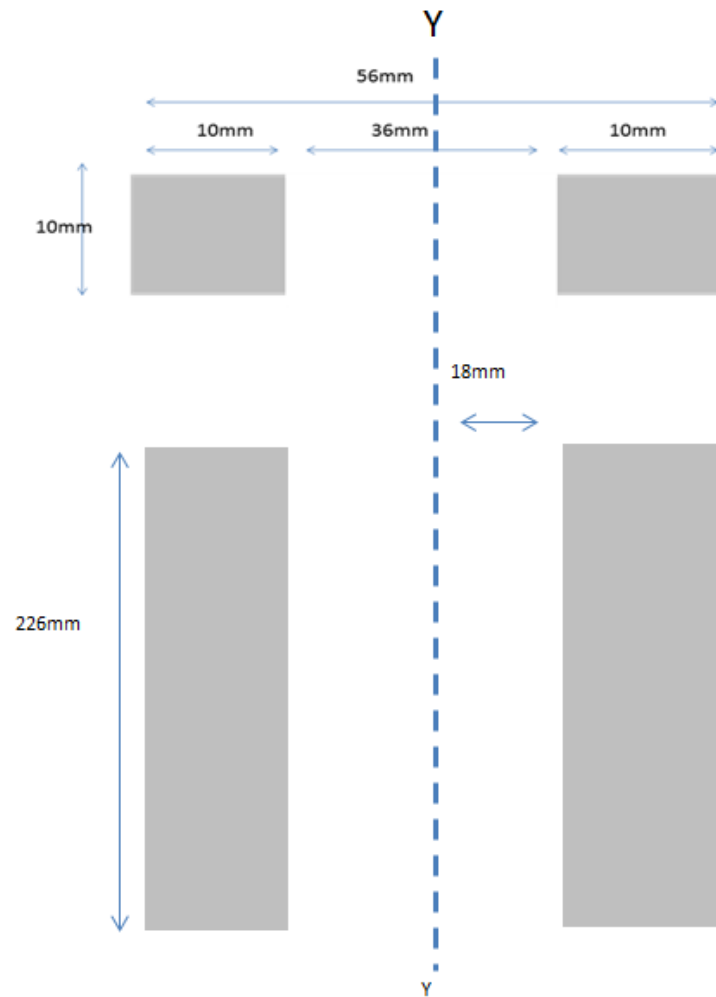
$$\sigma < \frac{yM}{I} \text{ where } M = \frac{Wab}{L}$$

$$W > \frac{\sigma IL}{aby}$$

$$W > \frac{130 \times 10^6 \times 1.66 \times 10^{-9} \times 0.226}{0.04 \times 0.186 \times 0.005}$$

$$W > 1.311 \text{ kN}$$

A.3.2 Front Bracket



$$I = 2 \times \left(\frac{0.01 \times 0.01^3}{12} + (0.01 \times 0.01 \times 0.023^2) \right)$$

$$I = 1.075 \times 10^{-7} \text{ m}^4$$

$$W > \frac{130 \times 10^6 \times 1.075 \times 10^{-7} \times 0.226}{0.04 \times 0.186 \times 0.028}$$

$$W > 15.16 \text{ kN}$$

Due to the front flipper bracket being lower in the chassis and the forces being directed horizontally have to be 15 times more than in the rear bracket.

A.3.3 Twisting of the flipper motor shaft

Upon disassembly of the flipper drive system it was found that the keyed motor shafts had sustained significant damage. Interestingly, the shafts had not worn – they had twisted. By examining the keyway the angle of twist was estimated to be around 5°. In order to establish the load that caused this damage the following equation can be used:

$$T = \frac{\theta J G}{L}$$

where T – torque applied ($N \cdot m$), θ – resulting angle of twist of the shaft (rad), J – polar 2nd moment of area, G – material shear modulus (Pa), L – length of the shaft in torsion (m) (School of Engineering 2008).

Polar 2nd moment of area for a round shaft can be calculated by:

$$J = \frac{\pi d^4}{32}$$

where d – diameter of the shaft (m).

So in this case it can be estimated that the 25mm long shaft 12 mm in diameter made out of carbon steel ($G = 77 \text{ GPa}$) has experienced a torque of:

$$T = \frac{0.087 \cdot 3.14 \cdot 0.012^4 \cdot 77 \cdot 10^9}{32 \cdot 0.025} = 543 \text{ N} \cdot \text{m}$$

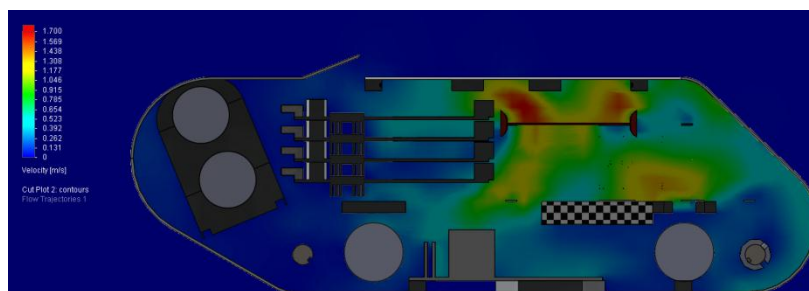
It should be noted that this is a conservative estimate of the peak load as the shaft has a tapered centre hole and a keyway that would reduce its real J value.

A.4 Thermal modelling results

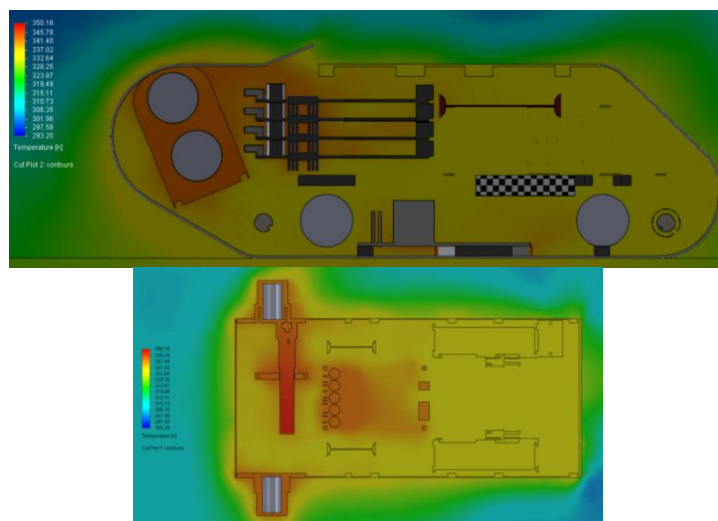
The following heat sources were modelled:

- Drive motors
- Power switching transistors on motor controller boards (with heatsinks)
- CPU (with small fan) and Northbridge (with heatsink) on computer board
- DC-DC power converters on power board (with heatsinks)

Single large fan



Maximum flow through motor controllers: 0 - 0.1 ms⁻¹

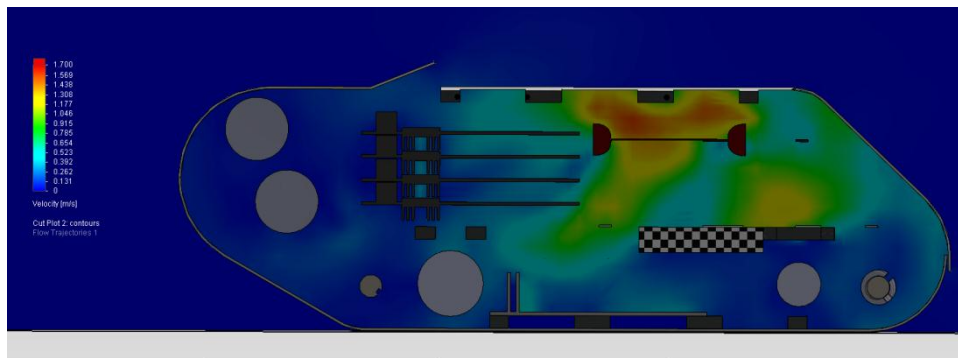


Motor controllers temperature: 72°C

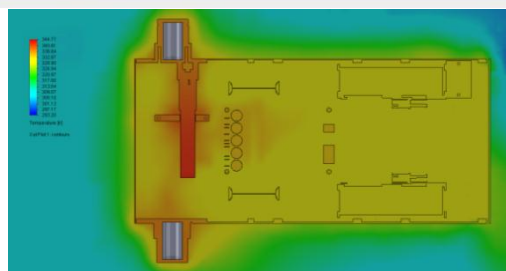
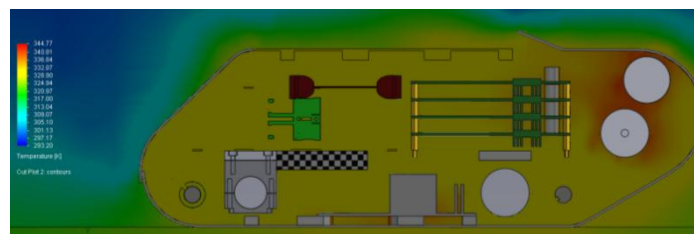
Drive Motors temperature: 77°C

This first iteration of the fan flow showed that air was being circulated in the front section of the robot, which is needed to cool the computer and power board. However there is minimal flow around the motors and the motor controllers, which lead the adding more fans to see if a better circulation could be generated.

Single large fan plus one extra to increase flow through motor controllers.



Maximum flow through motor controllers: 0.35ms^{-1}

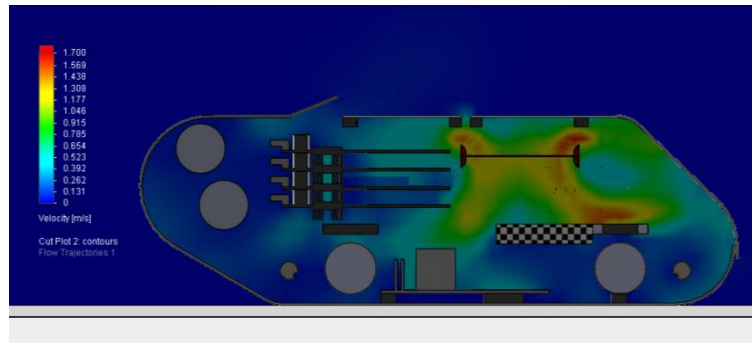


Motor controllers temperature: 64°C

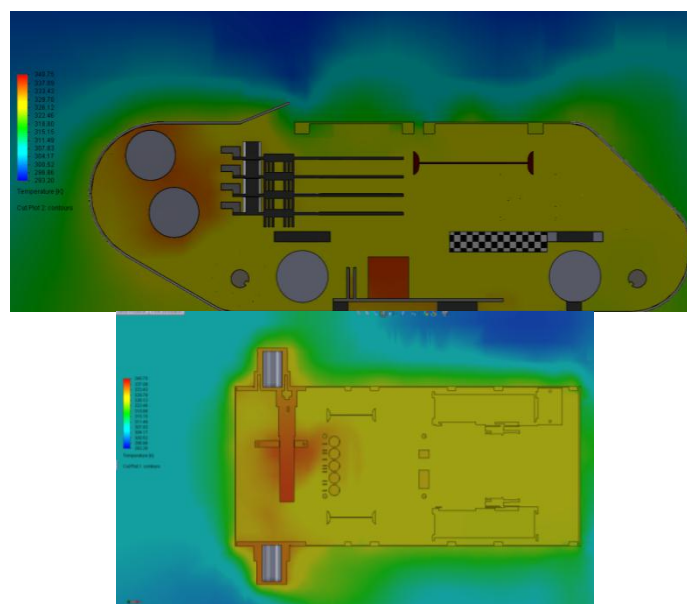
Drive Motors temperature: 71°C

The second fan was placed on parallel to the motor controllers, to pass air though the heat sinks, this increased the flow through the motor controllers but still the model showed no flow around the motors yet there was a cooling of 6°C which was noticed in the heat plot, when compared to the previous iteration.

Signal large fan plus two to increase flow through motor controllers.



Maximum flow through motor controllers: 0.5ms^{-1}



Motor controllers temperature: 53°C

Drive Motors temperature: 66°C

A third fan was added to the model to see if the flow in the entire robot could be increased. Ideally this fan would be placed facing the motors to help cooling however due to the lack of space, this fan was placed on the opposite side to the second fan. This increased the flow throughout the robot and cooled the motors and motor controllers by 11°C each. By using this configuration the air inside can be cooled on chassis walls using them as heat sinks, this means the if the model is correct no vents will need to be added to aid the cooling system.

A.5 Shell material selection

A number of materials were evaluated for the shell (Table 15). It is advantageous if the shell is light as this reduces the energy required to move the robot and helps save battery life. It must also be impact resistant as it will often come into contact with the environment, for instance, wooden blocks of the step fields. These have edges against which the robot internals must be protected. An additional requirement is that the shell can be manufactured easily and any modifications can be carried out in-house. Due to the uncertainty of using external suppliers for custom components precautions must be taken in case delivery is delayed or of poor quality.

Table 15. Advantages and disadvantages of the evaluated materials.

Material	Advantages	Disadvantages
Carbon fibre panels	Light	Expensive Difficult to shape in-house
Tegris polypropylene composite (Lankhorst Pure Composites b.v. 2013)	Light Impact resistant High strength	Impossible to shape in-house Expensive
Bamboo composites (Elmira 2013)	Very light	Strength could be insufficient Impossible to shape in-house Expensive
High Impact Polystyrene (HIPS)	Impact resistant Low melting point (can be shaped with a heat gun) Relatively cheap	Low yield strength
Acrylonitrile butadiene styrene (ABS)	Widely used (processing is well understood) Relatively cheap	Scratches easily

A number of material samples were ordered and tests were carried out (Figure 85). These included strength tests and bending using a heat gun.

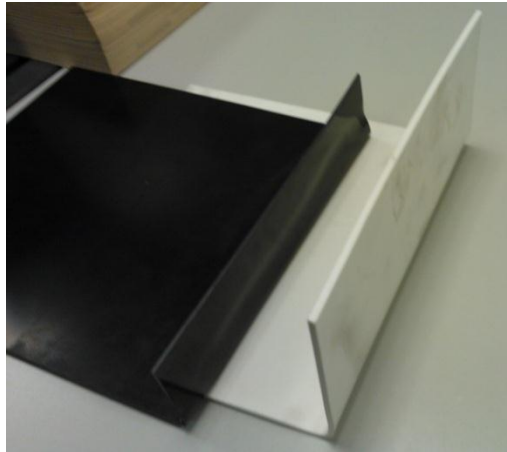


Figure 85. High Impact Polystyrene (HIPS) samples bent during testing using a heat gun.

As none of the team members had experience with these materials expertise was sought with academics (Youngblood 2012), composite component manufacturers (KS Composites 2013) and plastics fabricators (Bay Plastics Ltd. 2013). ABS and HIPS were shortlisted in favour of the more advanced materials due to the ease with which they can be shaped both at a supplier and in-house. The manufacturer (Bay Plastics) recommended the use of ABS over HIPS, so this was chosen as the final material.

A.5 Shell panel load calculations

To determine panel thickness a load case was set up where half of the weight of the robot (20 kg) is supported at one point in the middle of a 25 cm wide strip of ABS (Figure 86). It should be noted that this is a very pessimistic scenario as the shell is supported by the chassis along the most of the bottom of the robot.

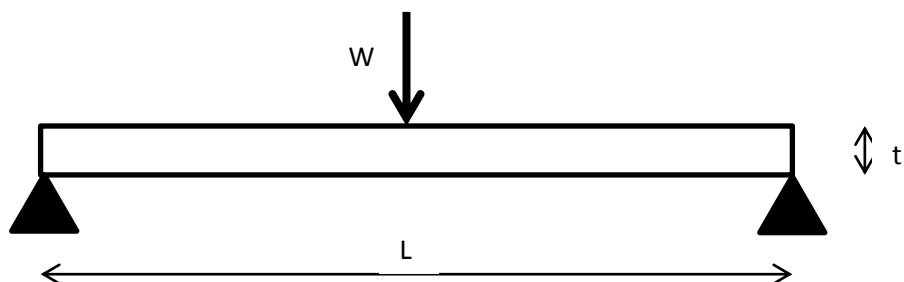


Figure 86. Load on a shell panel modelled as a simply supported beam. L – width of the robot, t – shell thickness, W – centrally applied load.

The stress induced in the material can be estimated using simple beam bending theory:

$$\frac{2\sigma}{t} = \frac{M}{I}$$

where σ – stress induced in the sheet (Pa), t – thickness of the sheet (m), M – moment applied (Nm), I – second moment of area of the cross section (m^4). The maximum moment arising due to a centrally applied load on a simply supported beam can be calculated by

$$M = \frac{WL}{4}$$

where W – force applied (N) and L – length of the unsupported section (m). The second moment of area for a rectangular cross section can be determined by

$$I = \frac{bt^3}{12}$$

where b – breadth of the section (m). Combining and rearranging the above equations an expression for the stress can be obtained:

$$\sigma = \frac{Mt}{2I} = \frac{WL \cdot t \cdot 12}{4 \cdot 2 \cdot bt^3} = \frac{3WL}{2bt^2}$$

Assuming a load of 20 kg (200 N) over the width of the robot of 250 mm for a sheet thickness of 2 mm and strip breadth of 250 mm the maximum stress induced in the material is:

$$\sigma = \frac{3WL}{2bt^2} = \frac{3 \cdot 200 \cdot 0.250}{2 \cdot 0.250 \cdot 0.002^2} = 75 \text{ MPa}$$

This is above the yield strength of ABS sheet (65 MPa (S&S 2013)). Increasing the sheet thickness to 3 mm:

$$\sigma = \frac{3WL}{2bt^2} = \frac{3 \cdot 200 \cdot 0.250}{2 \cdot 0.250 \cdot 0.003^2} = 33 \text{ MPa}$$

This results in a safety factor of 1.97 for a very unfavourable load case. Thus it can be assumed that a 3 mm thick ABS sheet will be sufficient to withstand loads seen in service.

Appendix B: Power System support materials

B.1 Wiring Diagram

Appendix C: Sensors & devices supporting data

C.1 Capability analysis of existing sensors

Table 16. Capability analysis of existing sensors.

Capability	Devices/ Sensors	Strengths	Weaknesses
Front and back real-time view	2x M1054 IP cameras (Axis Communications 2013)	<ul style="list-style-type: none"> • Low lag • Clear front and rear view of surroundings • High quality image • Cameras have built in LED lights 	<ul style="list-style-type: none"> • Occasional dropouts • Cameras are bulky
Two-way Communication	Axis M1054 IP camera – the front camera has 2-way audio	<ul style="list-style-type: none"> • Low lag • High quality audio 	
Controlling arm positions	3x servomotors: <ul style="list-style-type: none"> • A-Max 26 • A-Max RE-36 and • A-Max RE-30 (Maxon motor ag 2013) 3x potentiometers: <ul style="list-style-type: none"> • Vishay Model 357 (Vishay 2009) 	<ul style="list-style-type: none"> • Potentiometers measure absolute positions – suitable for inverse kinematics 	
Controlling flipper positions	2x relative encoders: <ul style="list-style-type: none"> • Maxon HEDL-5540 	<ul style="list-style-type: none"> • Flippers can be moved in incremental steps 	<ul style="list-style-type: none"> • Encoders relative not absolute – cannot keep track of flipper positions
Driving	Maxon RE-50	<ul style="list-style-type: none"> • Full range of mobility and speeds 	
Picking up objects	Off-the-shelf gripper powered by a HS-422 (Hitec 2013)	<ul style="list-style-type: none"> • Capable of picking up bottles of water and blocks with eyelets 	<ul style="list-style-type: none"> • Gripper not attached to robot
Heat detection	Photon 160 (FLIR Systems Co Ltd. 2012)	<ul style="list-style-type: none"> • Capable of detecting victim heat 	<ul style="list-style-type: none"> • Infrared camera not functional on robot

Breath detection	<ul style="list-style-type: none"> • Futurlec CO₂ sensor (Futurlec 2013) • Phidget board (Analogue-to-digital-converter) (Phidgets Inc. 2013) 	<ul style="list-style-type: none"> • CO₂ sensor in working condition 	<ul style="list-style-type: none"> • CO₂ sensor incorrectly powered in robot head – not functional
Mapping/ point cloud data	LiDAR module - Hokuyo URG-04LX (Hokuyo Automatic Co. 2009)	<ul style="list-style-type: none"> • LiDAR is functional • Capable of producing maps and point cloud data 	<ul style="list-style-type: none"> • LiDAR adds weight to the head • LiDAR attached to robot but unpowered • No mapping function on the client
Robot Orientation	Xsens MTi-28A53G35 (Xsens Technologies B.V. 2013)	<ul style="list-style-type: none"> • Capable of providing accurate orientation data 	<ul style="list-style-type: none"> • Xsens adds weight to the head • Xsens attached to the robot but unpowered • No orientation data sent to client
Head control – pan/ tilt	2x RX-64 servomotors (ROBOTIS 2010) using an RS-485 bus	<ul style="list-style-type: none"> • Pan and tilt of head is functional 	<ul style="list-style-type: none"> • Occasional dropouts of motors – power issue

Appendix D: Control system support materials

D.1 Inverse Kinematics – Flying the Head

The concept of flying the head is to move forwards, sideward and upwards based upon the direction the head is facing.

In order to do this, a local cylindrical co-ordinate frame ($r'-z'-\theta'$) is created on the joint by which the head rotates. This co-ordinate frame is in the same orientation as the global co-ordinate frame ($r-z-\theta$).

Assuming that the arm begins is the positions Δp_r and Δp_z and the user wants to move forward by a distance Δd , the change needed in both $r(\Delta p_r)$ and $z(\Delta p_z)$ can be calculated as follows.

Firstly, a solution is found in the cylindrical co-ordinate frame.

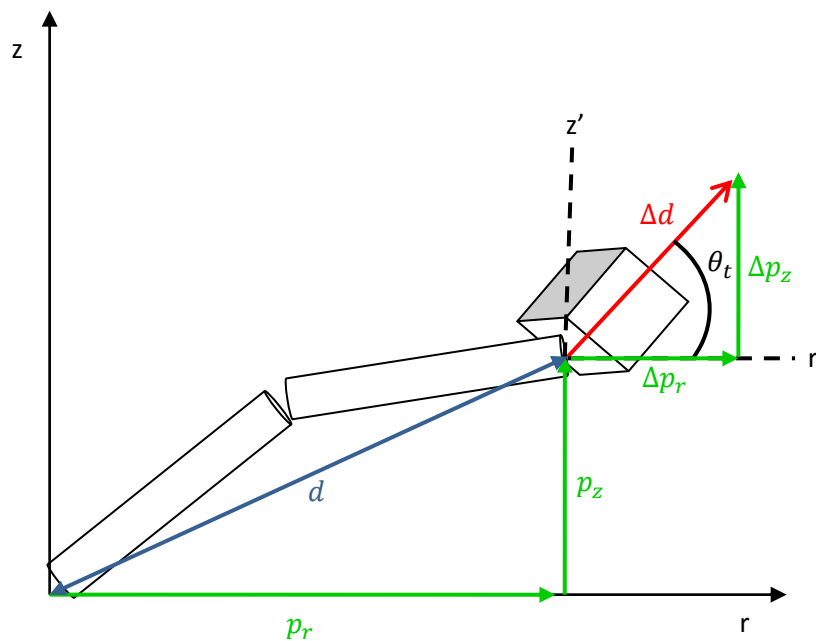


Figure 87 Robot arm in cylindrical coordinate frame

From this, Δp_z and Δp_r can be calculated in terms of the tilt angle θ_t ,

$$\Delta p_r = \Delta d \cos \theta_t$$

$$\Delta p_z = \Delta d \sin \theta_t$$

The cylindrical co-ordinate frame can now be transformed into a new Cartesian co-ordinate frame (x' - y' - z') using the pan angle θ_p (where p_x and p_y are the current arm co-ordinates in x and y respectively).

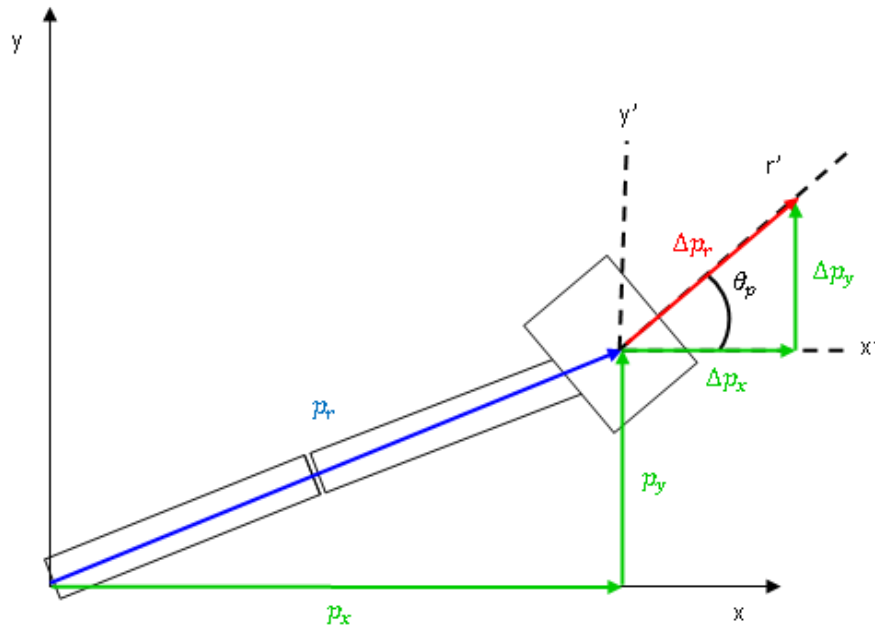


Figure 88 Robot arm top down view (x-y coordinate frame)

$$\Delta p_x = \Delta p_r \cos \theta_p$$

$$\Delta p_y = \Delta p_r \sin \theta_p$$

The Cartesian change in position can now be calculated in terms of the distance Δd , the pan angle θ_p , and the tilt angle θ_t

$$\Delta p_x = \Delta d \cos \theta_t \cos \theta_p$$

$$\Delta p_y = \Delta d \cos \theta_t \sin \theta_p$$

$$\Delta p_z = \Delta d \sin \theta_t$$

The final position based upon the previous position can now be calculated,

$$p_{x \text{ new}} = p_x + \Delta p_x$$

$$p_{y \text{ new}} = p_y + \Delta p_y$$

$$p_{z\ new} = p_z + \Delta p_z$$

These are the absolute positions that are configured in the code and then sent to the arm.

This completes the process for flying the head forwards. For flying sideward and upwards, the local co-ordinate frame on the end-effector is transformed using the appropriate rotation matrices.

D.2 Controller layout

The main controller layout is shown in Figure 89. Several different modes were used in order to fit all possible functions onto the one controller.



Figure 89. Main controller layout.

Drive Mode

The drive mode has been kept relatively the same as last year. This mode allows the user to control each track separately, like a tank and is very effective when attempting to navigate tight areas and step fields.



Figure 90. Drive mode controller layout (“tank” controls).

Inverse Kinematics Mode

The new inverse kinematics has been added as a separate arm control mode (Figure 91). This mode allows the user to ‘fly’ the head and is intended for delicate control of the arm such as pick and place operations or accurate positioning of the cameras for searching.



Figure 91. Inverse kinematics controller layout.

Search Mode

The aim of this mode was to replicate the controller layout familiar to most from shooting video games (Figure 92). This allows the user to move the arm and tracks at the same time and is useful for general driving of the robot and searching for victims in larger areas.

Up – raise arm up

Down – lower arm down

Left – fly head backward

Right – fly head forward



Control both tracks

Up/Down – Tilt head up/down

Left/Right – Pan head sideward

Figure 92. Search mode controller layout.

Joint-Control Mode

The ability to control each joint separately (Figure 93) was maintained this year as it has proved very useful in the past, especially when attempting to manoeuvre the arm into unusual and complicated positions.

Up – tilt head up

Down – tilt head down

Left – pan head left

Right – pan head right



Up/Down – Increase/decrease shoulder joint angle

Up/Down – Increase/decrease elbow joint angle

Left/Right – Rotate turret

Left/Right – Unused

Figure 93. Joint control mode layout

Appendix E: Other support materials

E.1 Remotec feedback

Peter Green

Programme and Future Development Manager
Northrop Grumman Corporation
Information Systems Europe
Remotec UK

29th April 2013 by email

Quote:

“The WMR system performed well for its first time out, there were concerns about its reliability however railway lines were negotiated with little effort followed by some off-roading and then stairs all within minutes of arrival.

The robot took some knocks and bumps and continuous vibration seen from track patter throughout the day and kept going proving to be robust.

The team had obviously spent some time building up the new chassis which looked together, and was easily accessible as it should be especially during the trialling period.

The team learnt that debris entering the track system will exert some forces on the chassis that static stress modelling will not show. A bracing bar to maintain the track drive train spacing may be needed as debris entering the track will locally bend the chassis rather than stretch the rubber track.

As the day went on driver confidence grew and negotiation of terrain and use of arm became second nature, again some valuable lessons were learnt here.

The Mimic ‘graphical model’ was very useful as the operator needed to know the orientation of his robot to ensure stability on a number of occasions.

The environmental situation awareness information was also useful to fill in the picture for the operator of distance and height which is often difficult to assess using 2d images from cameras alone.

We would suggest possibly overlapping the mimic with this so that the robot is seen as part of this overall sitrep rather than as a radar image, when the arm deploys the arm could be seen to avoid the walls as an example.”

E.2 Recommendations for further work

Chassis

- Design a method for keeping the tracks clear of debris
- A bracing bar to maintain the track drive train spacing may be needed as debris entering the track will locally bend the chassis rather than stretch the rubber track.
- Further weatherproofing – start by sealing shafts and making shell airtight
- Improve modulation of design – ensure each component is removable independently of other parts

Power System

- Fuses could be included as part of the housing instead of being located inside the robot. This would improve protection against the housing connector being short-circuited and make replacing fuses easier.
- The inward-facing surfaces for mounting electronics to the battery case leave a very small gap for wiring. Redesigning so that the electronics sit along one side of the housing would make wiring easier.
- The NFET disconnects the negative side of the battery, meaning the monitor's ground is no longer connected to the robot's ground and so the communication line between the two has to be isolated. A PFET solution would remove this requirement.
- Active balancing could be implemented to extend battery life.
- The mbed is not designed for low-power operation. Replacing it with a smaller microcontroller with a sleep mode would make the power board more efficient.
- The I²C switch used to provide 4 ports was difficult to source, finding an alternative or reducing the number of ports would solve this problem.

- A number of wires and connectors have a much higher current capacity than necessary. Using lower-spec components would reduce the size and weight taken up by wiring.
- Consider replacing the star-point ground with a second busbar to make rewiring easier.
- Try to have all connections to a system run through a single connector placed near that system to make disconnecting it simple.
- Investigate using SolidWorks Routing plug-in (Dassault Systemes 2012) to streamline wiring harness design process
- Redesign the motor controller boards to a smaller, standardised form factor. Keep all connectors on one side of the board for easier wire management.

Sensors and Devices

- Investigate longer range communication systems
- Reduce weight from the arm by replacing heavy aluminium components with lightweight alternatives
- Source a smaller computer

Control System

- Graceful communications failure – heartbeat or basic autonomy (return into radio coverage)
- Possible overlap of the 3D representation with the environmental situation information (e.g. LiDAR feedback) so the robot is seen as part of the overall site
- Investigate methods for autonomy – PieEye (08/09 report)
- Blob detection for the IR camera – could overlay onto webcam images

E.3 List of Abbreviations

ABS - Acrylonitrile butadiene styrene

DoF – Degrees of Freedom

FDM – Fused Deposition Modelling

FEA – Finite Element Analysis

GUI – Graphical User Interface

IC – Integrated Circuit

IK – Inverse Kinematics

IMU – Inertial Measurement Unit

IP – Internet Protocol

IR – infrared

LED – light emitting diode

LiDAR - Light Detection and Ranging

LiPo – Lithium Polymer Battery

NFET - Negative Channel Field Effect Transistor

PFET - Positive Channel Field Effect Transistor

PID – Proportional, Integral and Derivative control

PS3 – PlayStation 3

PWM – Pulse Width Modulation

QR – Quick Response code

RLLC – Robot Low Lag Connection

SLAM – Simultaneous Localisation and Mapping

SWOT – Strengths, Weaknesses, Opportunities, Threats

USAR – Urban Search and Rescue

USB – Universal Serial Bus

VLC – Video LAN Client

WMR – Warwick Mobile Robotics